AD NUMBER

ADB027191

LIMITATION CHANGES

TO:

Approved for public release; distribution is unlimited.

FROM:

Distribution authorized to U.S. Gov't. agencies only; Test and Evaluation; APR 1977. Other requests shall be referred to Air Force Armament Lab., Eglin AFB, FL 32542.

AUTHORITY

USADTC ltr 10 Apr 1980

A ROCKET ENGINE EXHAUST PLUME TEMPERATURE PROFILE BY LINE REVERSAL TECHNIQUE

AIR-TO-AIR MISSILES BRANCH
GUIDED WEAPONS DIVISION

APRIL 1977

FINAL REPORT FOR PERIOD
JULY 1976-NOVEMBER 1976

AIR FORCE ARMAMENT LABORATORY
AIR FORCE SYSTEMS COMMAND • UNITED STATES AIR FORCE
EGLIN AIR FORCE BASE, FLORIDA

REPORT DOCUMENTATION PAGE

READ INSTRUCTIONS BEFORE COMPLETING FORM

1. REPORT NUMBER	2. GOVT ACCESSION NO.	3. RECIPIENT'S CATALOG NUMBER
AFATL-TR-77-5[illegible]		

4. TITLE (and Subtitle)
A ROCKET ENGINE EXHAUST PLUME TEMPERATURE PROFILE BY LINE REVERSAL TECHNIQUE

5. TYPE OF REPORT & PERIOD COVERED
Final Report
Jul[illegible]-Nov[illegible]76

6. PERFORMING ORG. REPORT NUMBER

7. AUTHOR(s)
Jeffrey W. Griffin
Richard T. Schneider
William J. Rothschild

8. CONTRACT OR GRANT NUMBER(s)

9. PERFORMING ORGANIZATION NAME AND ADDRESS
Air-to-Air Missiles Branch
Guided Weapons Division
Air Force Armament Laboratory
Eglin Air Force Base, Florida 32542

10. PROGRAM ELEMENT, PROJECT, TASK AREA & WORK UNIT NUMBERS
Program Element: 62602F
JON: 1921[illegible]03 01

11. CONTROLLING OFFICE NAME AND ADDRESS
Air Force Armament Laboratory
Armament Development and Test Center
Eglin Air Force Base, Florida 32542

12. REPORT DATE
Apr[illegible]77

13. NUMBER OF PAGES
77

14. MONITORING AGENCY NAME & ADDRESS (if different from Controlling Office)
76p.

15. SECURITY CLASS. (of this report)
UNCLASSIFIED

15a. DECLASSIFICATION DOWNGRADING SCHEDULE

16. DISTRIBUTION STATEMENT (of this Report)
Distribution limited to U.S. Government agencies only; this report documents test and evaluation; distribution limitiation applied April 1977. Other requests for this document must be referred to the Air Force Armament Laboratory (DLMI) Eglin Air Force Base, Florida 32542.

17. DISTRIBUTION STATEMENT (of the abstract entered in Block 20, if different from Report)

18. SUPPLEMENTARY NOTES
Available in DDC

19. KEY WORDS (Continue on reverse side if necessary and identify by block number)
Hydrocarbon Exhaust Plume Characteristics
Air-to-Air Missiles and Target Systems
IR Signature
Optical Measurement of Plume Properties
Temperature Maps of Exhaust Plumes

20. ABSTRACT (Continue on reverse side if necessary and identify by block number)
This report contains temperature profile measurements of a small rocket engine burning RP-1 fuel. A standard line reversal technique with sodium as the emitting species was utilized. Apparent temperature maps of the engine plumes produced by oxygen-rich and fuel-rich mixture ratios in a stratochamber simulating altitude (pressure) conditions are also represented.

400 936

DD FORM 1 JAN 73 1473 EDITION OF 1 NOV 65 IS OBSOLETE

UNCLASSIFIED
SECURITY CLASSIFICATION OF THIS PAGE (When Data Entered)

Apparatus used for the measurements and calibration procedure are fully described in the report.

PREFACE

The work reported herein was conducted by the Air Force Armament Laboratory (AFATL) at Eglin Air Force Base, Florida, under Program Element 62602F, Project Number 19210301 as a part of the Infrared Technology Program. The work was performed in-house by the Infrared Technology Team of the Air to Air Missiles Branch during the period July 1976 to November 1976. By agreement between the AFATL and the University of West Florida, the data acquired and the experimental technique are also the subject of a masters' thesis for Mr. Jeffrey W. Griffin.

The authors wish to acknowledge the valuable assistance of Mr. Dale E. Fink and SSgt. Daniel Santo (DLMI).

This technical report has been reviewed and is approved for publication.

FOR THE COMMANDER

CLIFFORD H. ALLEN, JR., Colonel, USAF
Chief, Guided Weapons Division

(The reverse of this page is blank)

TABLE OF CONTENTS

Section	Title	Page
I.	INTRODUCTION	1
II.	THE MEASUREMENT METHOD	3
	1. Line Reversal Technique	3
	2. Temperature Unfolding Technique	6
	3. Determination of Concentration	9
III.	EXPERIMENTAL SET-UP	11
	1. Rocket Engine	11
	2. Optical Arrangement	12
IV.	EXPERIMENTAL RESULTS	15
	1. Temperature Measurements	15
	2. Relative Concentrations	16
References		39
Appendixes		
A	Determination of Species Concentration	41
B	Plume Temperature Unfolding Technique	44
C	Radial Temperature Scans	57

LIST OF FIGURES

Figure	Title	Page
1	Line Reversal Technique	18
2	Cross Section of Rocket Produced Plasma Field	19
3	Three Ring Division System	20
4	Ray Path Through Two Rings	21
5	Ray Path Through Three Rings	22
6	Imaging System	23
7	Oscilloscope Display for Sodium Doublet	24
8	Oscilloscope Displays for Pre- and Post-Reversal	25
9	Sample Data Set	26
10	Tungsten Lamp Calibration Curve	27
11	Filament Image Calibration Curve	28
12	Exhaust Plume	29
13	Centerline Temperature Distribution (O/F = 4.5)	30
14	Centerline Temperature Distribution (O/F = 4.5)	31
15	Radial Temperature Distribution (O/F = 4.5)	32
16	Unfolded Plume Temperature Distribution	33
17	Temperature Map of Plume	34
18	Relative OH Concentration Versus O/F Ratio	35
19	Relative CH Concentration Versus O/F Ratio	36
20	Relative C_2 Concentration O/F Ratio	37
21	Infrared Radiant Intensity Versus O/F Ratio	38

SECTION I

INTRODUCTION

The investigation of hydrocarbon exhaust plume characteristics is of interest to the Air Force for air-to-air missiles and target systems. IR seeker response during terminal guidance is at least partially determined by the spatial distribution of plume radiation.

The optical and IR signature of the plume is determined by the temperature distribution and the characteristic frequencies (spectrum lines) of the radiating species. The radiating species are the combustion products and radicals formed by the chemical reactions in the rocket plume. For this reason, experimental determination of these properties is of utmost importance. In addition, reliable analytical models of hydrocarbon rocket or jet engine plumes need to be developed to predict the behavior of new or unknown engine designs.

Optical measurement of plume properties (temperature and intensities) is mandatory for the validation of these models. Another way to check these models is to measure the concentration of the combustion products and radicals formed in the rocket plume and the relative changes in concentration of these species if the oxygen to fuel (O/F) ratio is changed. This information can also be obtained by spectroscopic measurements. Consequently, the primary objective of this project was to produce temperature maps of the exhaust plume generated by a small rocket engine burning RP1 with gaseous O_2 as the oxidizer. After having obtained the temperature distributions, previous measurements of spectral intensities of radicals could be converted into relative changes in concentration as a function of oxygen to fuel ratio. The method chosen for the temperature measurements was the line reversal technique with sodium used as the emitting species. The temperatures obtained with such a technique are most accurate when obtained from a homogeneous plasma of constant temperature, density, and species concentration. When such conditions are not met (such as in rocket exhaust plumes) the measurements produce an average temperature due to the existence of temperature gradients. Techniques are proposed for unfolding these average temperature profiles to produce corrected radial temperature distributions of the plume. The investigations reported here are the first experimental application of these techniques to a rocket plume.

Average temperature maps were made of plumes produced by both oxygen-rich (O/F = 4.5) and fuel-rich (O/F = 2) mixture ratios. For the oxygen-rich conditions (O/F = 4.5) both radial centerline temperature measurements were made.

A corrected (unfolded) radial temperature distribution was generated for one plume cross section at the O/F = 4.5 condition. The unfolded temperature profile was compared with the average temperature profile obtained at the same location. This procedure provides an estimate of the error incurred in applying standard line reversal techniques to non-homogeneous rocket plumes.

Due to unstable burning conditions and poor plume definition at the fuel-rich mixture ratio (O/F =2) only a centerline temperature distribution was produced. However, the experience gained with unfolding of the O/F = 4.5 temperature profile makes it possible to estimate the true temperature of these measurements even without undergoing an unfolding procedure.

SECTION II

THE MEASUREMENT METHOD

1. LINE REVERSAL TECHNIQUE

For a homogeneous plasma in thermodynamic equilibrium, the radiation field is given by

$$I_\lambda = B_\lambda^P(T) = \frac{2hc_o^2}{\lambda^5} \frac{1}{\exp(hc_o/\lambda kT)-1} \qquad (1)$$

where $B_\lambda^P(T)$ is the Planck function and T is the plasma temperature.

In case of complete thermodynamic equilibrium, the plasma is a blackbody and its radiation is only a function of surface area and temperature. It is not a function of any material constants. A rocket plume is not such a radiator, it is only local in thermodynmaic equilibrium (LTE). In this case, the radiation is determined by the volume of the plasma, its temperature and a materials constant, usually expressed as an absorption coefficient. Consider a homogeneous slab of plasma in local thermodynamic equilibrium (LTE) as indicated in Figure 1. At any given point inside this plasma the radiation field is determined by two competing factors. The plasma emits energy of amount ε_λ erg/cm^3 sec per unit wavelength, where ε_λ is the emission coefficient. It also absorbs energy at the rate $k(\lambda)I_\lambda(r)$ where $k(\lambda)$ is the absorption coefficeint of the plasma at a particular wavelength and $I_\lambda(r)$ is the radiation intensity of some position r in the plasma slab. The rate of change of intensity through the slab is a function of these two competing terms and is, obviously, given by their difference

$$\frac{dI_\lambda(r)}{dr} = \varepsilon_\lambda - k(\lambda)I_\lambda(r) \qquad (2)$$

It is assumed that the plasma slab under consideration is homogeneous, which means that temperature, emission coefficient and absorption coefficient are not a function of r. Of course, this is only an initial assumption for discussion of the method. In a real plasma, like a rocket plume, these properties are indeed a function of r. In this case, it will be necessary to divide the plume into rings small enough that it can be assumed that within one ring the plasma is homogeneous.

The assumption of LTE requires that Kirchoff's Law is valid. Kirchoff's Law establishes a connection between ε_λ and k (λ). It states that the ratio of emission coefficient to the absorption coefficient is only a function of temperature and is equal to the Planck function. The result being that

$$\varepsilon_\lambda = k(\lambda) B_\lambda^P(T). \qquad [B_\lambda^P(T) \text{ Planck function of the plasma}] \tag{3}$$

Inserting this result into equation (2) yields

$$\frac{dI_\lambda(r)}{dr} = k(\lambda) B_\lambda^P(T) - k(\lambda) I_\lambda(r) \tag{4}$$

or

$$\frac{dI_\lambda(r)}{dr} = k(\lambda) [B_\lambda^P(T) - I_\lambda(r)] \tag{5}$$

This may be integrated utilizing a change of variable

$$B_\lambda^P(T) - I_\lambda(r) = K \tag{6}$$

or

$$I_\lambda(r) = B_\lambda^P(T) - K \tag{7}$$

and

$$dI_\lambda(r) = -dK \tag{8}$$

Inserting equation (6) and equation (8) into equation (5) we have

$$-\frac{dK}{dr} = k(\lambda) K \tag{9}$$

or

$$\frac{dK}{K} = -k(\lambda) dr \tag{10}$$

Integration of equation (10) produces

$$\int_{K_o}^{K} \frac{dK}{K} = -k(\lambda) \int_o^r dr \tag{11}$$

or

$$\ln K = -k(\lambda) r + \ln K_o \tag{12}$$

and

$$K = Ce^{-k(\lambda) r} \tag{13}$$

where

$$K_o = C \tag{14}$$

Utilizing equation (6) yields

$$I_\lambda(r) = B_\lambda^P(T) - Ce^{-k(\lambda) r} \tag{15}$$

Letting $I_\lambda(r) = I_{\lambda,o}$ at $r = 0$, C may be evaluated

$$C = B_\lambda^P(T) - I_{\lambda,o} \tag{16}$$

Finally, inserting equation (16) into equation (15) yields

$$I_\lambda(r) = B_\lambda^P(T) - [B_\lambda^P(T) - I_{\lambda,o}]\, e^{-k(\lambda)r} \tag{17}$$

or

$$I_\lambda(r) = B_\lambda^P(T)[\,1 - e^{-k(\lambda)r}] + I_{\lambda,o}\, e^{-k(\lambda)r} \tag{18}$$

In the technique of line reversal temperature measurement a standard illumination source is imaged upon the boundary of the plasma field. The image of the source is calibrated against a standard blackbody, thereby giving an quivalent brightness temperature for the illuminating radiation $I_{\lambda,o}$ in Figure 1. The incident radiation intensity can thereby be given as

$$I_{\lambda,o} = B_\lambda^S(T) \tag{19}$$

where $B_\lambda^S(T)$ is the Planck function for the source image. The temperature of the standard source is adjusted until the output intensity equals the incident intensity or

$$I_\lambda(r) = B_\lambda^P(T)\ [\,1 - e^{-k(\lambda)r}] + B_\lambda^S(T)e^{-k(\lambda)r} = B_\lambda^S(T) \tag{20}$$

for $r = \ell$ we have

$$B_\lambda^S(T) = B_\lambda^P(T)\ [\,1 - e^{-k(\lambda)\ell}] + B_\lambda^S(T)e^{-k(\lambda)\ell} \tag{21}$$

the final result being that

$$B_\lambda^S(T) = B_\lambda^P(T) \tag{22}$$

Since the Planck function is a function only of temperature, this implies that the plasma and source image temperature are equal

$$T_P = T_S \tag{23}$$

The above technique is correct only for homogeneous slabs in local thermodynamic equilibrium. In other words, the states of atoms or molecules emitting the wavelength region which is used for the line reversal technique have to be excited according to a Maxwell-Boltzmann distribution. For a good precision of the measurement it is also required that the absorption coefficient is of a certain minimum value. Although the absorption coefficient is not explicitly measured, the method depends on the fact that absorption takes place in the plasma [see Equation (2)].

Absorption requires that the lower state of the spectrum line used for the method is appreciably populated. This can be guaranteed best by using as the lower state the ground state of the atom. For this reason mostly resonance lines are used for the line reversal method. Only a few chemical elements have resonance lines in the visible spectrum region (e.g., Na, K,).

2. TEMPERATURE UNFOLDING PROCEDURE

Temperatures are not additive. Therefore, if a temperature gradient exists, regular Abel unfolding techniques which are based on the fact that intensities are additive cannot be used.

However, the quantity $t = k \cdot \ell$, sometimes referred to as an optical length, is additive. A temperature unfolding technique can be based on this fact.

Therefore, a radial temperature distribution may be obtained by dividing the plume cross section into thin concentric homogeneous rings. Figure 2 illustrates such a division where a three-ring section is utilized. Each ring is assumed to contain a homogeneous plasma with Planck funtion $B_\lambda^{Pn}(T)$ and absorption coefficient $k_n(\lambda)$. This assumption requires the existence of LTE with Kirchoff's Law being valid in a narrow spectral range. The accuracy of such a layering technique is, of course, dependent upon the thickness of the slabs, therefore Δ is kept small.

The calculation of the $B_\lambda^{Pn}(T)$ is straightforward, provided the outermost ring temperature is known. This temperature may be obtained by a line reversal temperature measurement. The method of determining the remaining $B_\lambda^{Pn}(T)$ is now explained.

For simplicity, consider a plasma divided into three rings as seen in Figure 3. Consider incident radiation of intensity I_{λ,o_n}. The total intensity on the right side of the plasma is I_{T_n} Let I_{P_n} be the intensity of radiation emitted by the plasma itself. Then

$$I_{T_n} = I_{P_n} + I_{\lambda,o_n} e^{-\tau_n} \tag{24}$$

where τ_n is the optical thickness of the plasma for a given path and is given by

$$\tau_n = 2 \sum_{m=1}^{n} k_m(\lambda) \ell_{n,m} \tag{25}$$

For the outermost ray (outside ring only traversed) we have that

$$I_{T_1} = I_{P_1} + I_{\lambda,o} e^{-\tau 1} \tag{26}$$

where

$$\tau_1 = 2k_1(\lambda)\ell_{1,1} \tag{27}$$

or

$$k_1(\lambda) = \frac{1}{2\ell_{1,1}} \ln\left[\frac{I_{\lambda,o_1}}{I_{T_1} - I_{P_1}}\right] \tag{28}$$

The intensities in equation (28) are easily determined and $\ell_{1,1}$ is measureable from the plume geometry. Knowing $k_1(\lambda)$ the remaining $k_n(\lambda)$ may be determined.

$$k_2(\lambda) = \frac{1}{2\ell_{2,2}} \ln\left[\frac{I_{\lambda,o_2}}{I_{T_2} - I_{P_2}}\right] - \frac{k_1(\lambda)\ell_{2,1}}{\ell_{2,2}} \tag{29}$$

where

$$\tau_2 = 2[k_2(\lambda)\ell_{2,2} + k_1(\lambda)\ell_{2,1}] \tag{30}$$

and

$$k_3(\lambda) = \frac{1}{2\ell_{3,3}} \ln\left[\frac{I_{\lambda,o_3}}{I_{T_3} - I_{P_3}}\right] - \left[\frac{\ell_{3,1}k_1(\lambda) + \ell_{3,2}k_2(\lambda)}{\ell_{3,3}}\right] \tag{31}$$

where

$$\tau_3 = 2[\ell_{3,1}k_1(\lambda) + \ell_{3,2}k_2(\lambda) + \ell_{3,3}k_3(\lambda)] \tag{32}$$

The problem now remains to calculate the $B_\lambda^{P_n}(T)$. As stated earlier, the temperature and thereby the Planck function of the outer ring are determined through line reversal measurements. Therefore $B_\lambda^{P_1}(T)$ is known.

Consider now the ray that passes through the outer two rings (Figure 4). Inside the first ring the intensity may be written as

$$I(r_1) = B_\lambda^{P_1}(T)\left[1 - e^{-k_1(\lambda)r_1}\right] + I_{\lambda,o_2}e^{-k_1(\lambda)r_1} = A \text{ for } r_1 = \ell_{2,1} \tag{33}$$

Inside the second ring we have

$$I(r_2) = B_\lambda^{P_2}(T)\left[1 - e^{-k_2(\lambda)r_2}\right] + A\, e^{-k_2(\lambda)r_2} = B \text{ for } r_2 = 2\ell_{2,2} \tag{34}$$

On the far side again in the first ring we have

$$I(r_3) = B_\lambda^{P1}(T)\ [\,1 - e^{-k_1(\lambda)r_3}] \ + \ B\, e^{-k_1(\lambda)r_3} \tag{35}$$

At reversal for $r_3 = \ell_{2,1}$ we have

$$I(r_3) = I_{\lambda,o_2} = B_\lambda^{S2}(T) \tag{36}$$

where $B_\lambda^{S2}(T)$ is the Planck function for the source image. Since the objective of this technique is to improve upon line reversal temperature measurements the $B_\lambda^{Sn}(T)$ are known from previously generated average temperature profiles. So we have that

$$\begin{aligned} B_\lambda^{S2}(T) = {} & B_\lambda^{P1}(T)\ [\,1 - e^{-k_1(\lambda)\ell_{2,1}}] \\ & + \Big[B_\lambda^{P2}(T)\ \{1 - e^{-2k_2(\lambda)\ell_{2,2}}\} \\ & + \{B_\lambda^{P1}(T)\ [\,1 - e^{-k_1(\lambda)\ell_{2,1}}] \\ & + B_\lambda^{S2}(T) e^{-k_1(\lambda)\ell_{2,1}}\}\ e^{-2k_2(\lambda)\ell_{2,2}} \Big]\ e^{-k_1(\lambda)\ell_{2,1}} \end{aligned} \tag{37}$$

This may be solved for $B_\lambda^{P2}(T)$ and we have

$$B_\lambda^{P2}(T) = \left[\left\{ \frac{B_\lambda^{S2}(T) - B^{P1}(T)\ [1 - e^{-k_1(\lambda)\ell_{2,1}}]}{e^{-k_2(\lambda)\ell_{2,1}}} \right\} \right.$$

$$\left. - \frac{\{B_\lambda^{P1}(T)\ [1 - e^{-k_1(\lambda)\ell_{2,1}}] + B_\lambda^{S2}(T) e^{-k_1(\lambda)\ell_{2,1}}\}\ e^{-2k_2(\lambda)\ell_{2,2}}}{[1 - e^{-2k_2(\lambda)\ell_{2,2}}]} \right] \tag{38}$$

Since the Planck function is a function of temperature only, the temperature of the second ring is determined. The process is cascading one, i.e., each consecutive ring temperature requires all of the outer ring temperatures. For the path through three rings we have (Figure 5)

$$I(r_1) = B_\lambda^{P1}(T)\ [\,1 - e^{-k_1(\lambda)r_1}\,] \ + I_{\lambda,o_3} e^{-k_1(\lambda)r_1} = A \text{ for } r_1 = \ell_{3,1} \tag{39}$$

$$I(r_2) = B_\lambda^{P2}(T)\ [\ 1 - e^{-k_2(\lambda)r_2}\ ]\ + A\ e^{-k_2(\lambda)r_2} = B \text{ for } r_2 = \ell_{3,2} \quad (40)$$

$$I(r_3) = B_\lambda^{P3}(T)\ [\ 1 - e^{-k_3(\lambda)r_3}\ ]\ + B\ e^{-k_3(\lambda)r_3} = C \text{ for } r_3 = 2\ell_{3,3} \quad (41)$$

$$I(r_4) = B_\lambda^{P2}(T)\ [\ 1 - e^{-k_2(\lambda)r_4}\ ]\ + C\ e^{-k_2(\lambda)r_4} = D \text{ for } r_4 = \ell_{3,2} \quad (42)$$

and finally

$$I(r_5) = B_\lambda^{P1}(T)\ [\ 1 - e^{-k_1(\lambda)r_5}\ ]\ + D\ e^{-k_1(\lambda)r_5} = E \text{ for } r_5 = \ell_{3,1} \quad (43)$$

For the reversal condition we have

$$E = B_\lambda^{S3}(T) \quad (44)$$

and

$$B_\lambda^{P1}(T)\ [\ 1 - e^{-k_1(\lambda)\ell_{3,1}}]\ + D\ e^{-k_1(\lambda)\ell_{3,1}} = B_\lambda^{S3}(T) \quad (45)$$

This equation contains one unknown, namely $B_\lambda^{P3}(T)$. Thus it can be seen that the ring temperatures can be determined by the above procedure. The technique can be extended to any number of rings desired.

3. DETERMINATION OF CONCENTRATIONS

As pointed out in the introduction the measurement of concentrations of radiating species provides insight into the chemistry of the rocket plume. In case of atomic species, if a Maxwell-Boltzmann distribution of states exists, the intensity density of an emission line of a spectrum line can be related to the particle density n_o (and so to the concentration) by:

$$I = n_o \frac{g}{U} h\nu\ Ae^{-\frac{E}{KT}} \quad (46)$$

where

g = statistical weight or degeneracy of the upper state of the line

A = transition probability

$h\nu$ = energy of the photon

U = partition function

E = excitation energy of the line

K = Boltzmann factor

T = temperature.

If the temperature is known, measurement of the intensity will produce a value for n_o, since all the other quantities in equation (46) are known atomic constants. Measurement of relative change of intensity for a changing O/F ratio in the rocket plume can be interpreted in terms of the relative change in concentration of a certain species, again under the assumption that the temperature has been measured by some means (e.g., the line reversal method). The complete technique is described in Appendix A.

Most of the radiating species in the rocket plume are, however, molecules or radicals. In this case a modified form of equation (46) which gives the intensity of a line in a rotational band must be used.

$$I \propto (2J + 1) e^{\frac{-J\,(J+L)h}{8\pi^2\,\Theta KT}} \qquad (47)$$

where

J = rotational Quantum number

$\Theta = mr^2$ (m = mass of molecule

r = intermolecular separation distance)

h = Planck's Constant

SECTION III
EXPERIMENTAL SET-UP

1. ROCKET ENGINE

The experiment described in this report was conducted at the Range 22 Stratochamber Test Facility at Eglin Air Force Base. The capabilities of this installation are described in Reference 1. The experimental apparatus consisted of a small kerosene/gaseous oxygen rocket which exhausted into a vacuum chamber, a sodium injection system, a standard illumination source, an imaging optical system, and a spectroscopic measurement system.

The rocket engine used in the experiment was a small kerosene/gaseous oxygen rocket that is based on an original design by Astrosystems, Inc., Lake Success, New York. The rocket engine injector essentially consists of a cylinder with a 0.055-inch-diameter orifice. Gaseous oxygen is introduced into the injector upstream of the kerosene and at a higher pressure than the kerosene. This design permits mixing and atomization to occur prior to injection into the combustion chamber. In the wall of the combustion chamber is a port for injection of seed material (sodium chloride) into the plume for application of the line reversal technique. Typical chamber pressure is 40 psi requiring that the seed supply line be pressurized at a higher value (80 to 100 psi).

The engine was mounted on a horizontal/vertical translator which was electronically controlled outside of the chamber during data runs. The translator was capable of engine movements of 1 mm increments along both axes. Associated with the rocket engine was the control panel and flow hardware. Precision micrometer values located in the respective lines permitted the fuel and oxygen flow rates to be adjusted to achieve a desired oxygen to fuel ratio during operation of the engine. The combustible mixture is initially ignited by a spark plug. Total mass flow for the engine was maintained at 5 grams per second. For the O/F = 2

condition, the flow rates were oxygen 3.33 grams per second, RP1 1.67 grams per second and for O/F = 4.5, oxygen 4.10 grams per second, RPI 90 grams per second.

A sodium chloride/water solution of 47 grams per liter was used as the plume seed material. The solution was force-fed to the engine through a 0.25 inch copper line from a nitrogen pressurized steel tank. Tank pressure ranged from 80 to 100 psi. Metering was accomplished by a precision micrometer needle valve. To facilitate metering, a 0.018-inch-diameter orifice was placed ahead of the combustion chamber port. The orifice also acted as an atomizer for the sodium chloride solution and prevented extinction of the plume by excess water. Consistent sodium chloride injection was insured by constant monitoring of combustion chamber pressure and maintenance of this pressure at approximately 40 psi.

2. OPTICAL ARRANGEMENT

The objectives of the optical imaging system were to (1) image a tungsten ribbon lamp filament upon the rocket plume centerline with a magnification ratio equal to unity, and (2) image the plume and filament upon the entrance slit of the spectrometer with a convenient magnification ratio. A schematic diagram of the imaging system is shown in Figure 6.

The tungsten filament was imaged by a telephoto astigmat lens with an effective focal length of 20 inches and f-number of 5.6. Unity magnification required that the filament be located a distance of (2) x (effective focal length) from the principal plane of the lens. Verification of correct distances is accomplished by accurately measuring the filament size and adjusting the optics to obtain unity magnification.

The filament image and plume were imaged onto the spectrometer entrance slit by a 12-inch-diameter parabolic mirror of focal length 2.51 meters. This is facilitated by folding the beam with a 12-inch-diameter plane front surface mirror. The plume and filament image are slightly magnified by this system with a magnification ratio of 1.05. The spectrometer used was a 0.75 meter Czerny-Turner mount (manufacturer: Jarrell-Ash).

The spectrometer was equipped with a 148-groove/mm grating blazed for 5 microns.

A 500-element silicon multichannel detector unit was mounted at the exit plane of the spectrometer and the grating rotated to allow illumination of the detector array by the sodium doublet (approximately 5890Å). The multichannel detector unit was interfaced with an Optical Multichannel Analyzer (OMA). The OMA (manufacturer: Princeton Applied Research) allowed real time display of relative incident intensities upon the silicon detector array via oscilloscope interfacing, as indicated in Figure 7.

Such relative intensity displays could be stored in the OMA memory unit and plotted for permanent record with an X-Y plotter.

Figure 8 shows a typical output of the X-Y plotter for pre-reversal and post-reversal conditions. Figure 9 shows how actual reversal was established. Once a reversal condition was established (center part of Figure 9) the lamp temperature was increased slightly (upper part of Figure 9) and decreased slightly (lower part of Figure 9) until a distinct signal could be detected. In the case of Figure 9, this required an increase or decrease of the shunt voltage drop by 0.04 mV. This translates into change in temperature of $\pm 6^{\circ}K$. The sensitivity of the method, which is the relative error, is therefore better that this value.

The standard light source consisted of a calibrated tungsten ribbon lamp with its associated variable high current dc power supply. A precision shunt was inserted in series with the lamp filament and the voltage drop across the shunt was monitored by a dc micro-voltmeter. This allowed calibration of the lamp with an optical pyrometer, the result being establishment of a relationship between shunt voltage and filament brightness temperature. The calibration curve is shown in Figure 10.

As pointed out above, in the line reversal technique the tungsten ribbon lamp filament is imaged onto the boundary of the plasma field produced by the rocket plume. The filament image thereby becomes the new standard source for experimental measurements. This necessitates calibration of the filament image with an optical pyrometer.

The resultant calibration curve which relates the shunt voltage of the filament of the standard lamp to the brightness temperature of the filament image at the centerline of the plume is shown in Figure 11. This calibration curve is slightly different from Figure 10, due to the fact that the standard lamp radiation experiences a slight absorption at window No. 1 when entering the vacuum chamber. Of course, there is also some absorption in window No. 2. But, since both the light coming from the standard lamp and light coming from the plume are absorbed in the same way, the influence of window No. 2 cancels and the temperature measurement is not affected.

SECTION IV

EXPERIMENTAL RESULTS

1. TEMPERATURE MEASUREMENTS

A photograph of the exhaust plume is shown in Figure 12. There is a visible shock structure which corresponds quite will to the structure observed in the temperature scans.

These results are shown in Figures 13 and 14. The spatial resolution of the measurement setup was 1 mm. Figure 13 is a plot of the centerline temperature of the plume for an O/F = 4.5, which is a lean mixture. The nozzle exit temperature was found to be $T_{ex} = 2503^{o}K$, which compares very well with the theoretical prediction of $T_{ex} = 2570^{o}K$ reported by Vamos (Reference 2). The temperature rises in the front of each shock drastically (from $1825^{o}K$ to $2245^{o}K$ within 1 mm at the first shock front) and decreases to a temperature of $T = 1827^{o}K$ which is fairly uniform between all shocks. Figure 14 shows the same measurement for an O/F = 2.0 (rich mixture). The temperatures are, in general, lower and the temperature rise in the shock front is not nearly as pronounced as in the O/F = 4.5 case. These findings have to be compared to Figures 18, 19, and 20, which indicate increased formation of radicals with increasing richness of expense the fuel mixture. This means formation and excitation of the radicals at the expense of random energy of the plume proper.

The line reversal measurements indicate that the plume exhibits a moderate temperature gradient in the radial direction. A reversal temperature profile for one cross section at the O/F = 4.5 condition is shown in Figure 15. This profile was unfolded to produce a true radial temperature distribution which is shown in Figure 16. A full discussion of the unfolding technique including actual data and a computer program for numerical evaluation of the data are contained in Appendix B. A large number of cross sections were scanned and this material is compiled in Appendix C. From this material a temperature map of the plume was

constructed for the case of O/F = 4.5. This map is shown in Figure 17. Since the radial temperature gradients were moderate, the correction obtained by the unfolding process was less than 30 percent. However, the precision of the line reversal technique for the temperature range of interest for this investigation is ±1 percent. Therefore, the corrections resulting from this unfolding process seem very worthwhile.

2. RELATIVE CONCENTRATIONS

The visible and ultraviolet spectra were obtained in the rocket plume previously (Reference 3). The observed spectra were those of the radicals OH, CH, and C_2 (Swan and higher pressure bandhead at 5165Å). The relative intensity of these bands was measured as a function of oxygen to fuel mixture ratio. In all cases, an extremely sharp increase in band intensity occurs when the mixture ratio is reduced below O/F = 3.5 (stoichiometric) and reaching a maximum at O/F = 1.8. The same behavior is found for the total CO_2 in the 4-to 5-micrometer infrared emission band. These data show that the plume radiation is primarily due to external combustion between fuel-rich exhaust products and air.

The obtained relative intensities were converted into relative concentrations using the reported temperatures. Details of the conversion technique are contained in Appendix A. The results based on the above three bandhead wavelengths are shown in Figures 18, 19 and 20. In all cases, an extremely sharp increase in band radiation intensity occurs as the O/F ratio is reduced below 3.5 (stoichiometry). This variation with O/F ratio is similar to that observed in molecular CO_2 emission in the infrared band between 4 and 5 microns, although the rate of increase in visible band radiation is much larger. The previously measured (Reference 3) infrared radiant intensity variation with mixture ratio is reproduced in Figure 21 to show the comparison.

The presence of strong C_2 and CH emission are indicators of fuel-rich flame combustion. Their concentrations begin to fall off below a mixture ratio of 1.8, as does the infrared radiant intensity, indication that the threshold for carbon luminosity may have been reached. However, although

carbon soot is visually evident in the exhaust of engines under these fuel-rich conditions, it is apparent that the amount is nonetheless not high enough to contribute significant infrared radiation.

The data thus show the rocket engine radiation to be primarily due to external combustion. An increase in infrared radiation accompanies the increase in visible radiation, i.e., the increase in external combustion. No graybody radiation is present in the infrared spectrum under these conditions (Reference 3) and only a limited visible continuum was observed over the shock regions.

OH radical was determined to be the major plume emitter at visible and ultraviolet wavelenghts at high mixture ratios and beyond the region of the shocks. None of the major molecular combustion products, such as H_2O, CO_2, or CO, some of which are primary infrared radiators, were observed to emit in the visible or ultraviolet. The O/F ratio, as in the infrared wavelengths, is the predominant parameter affecting the intensity and spectrum of OH radiation in the UV.

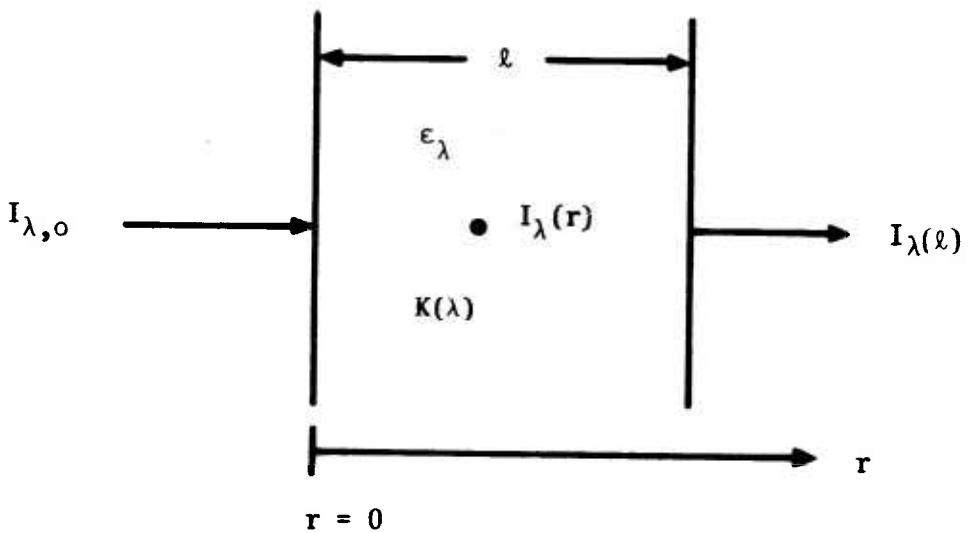

Figure 1. Line Reversal Technique

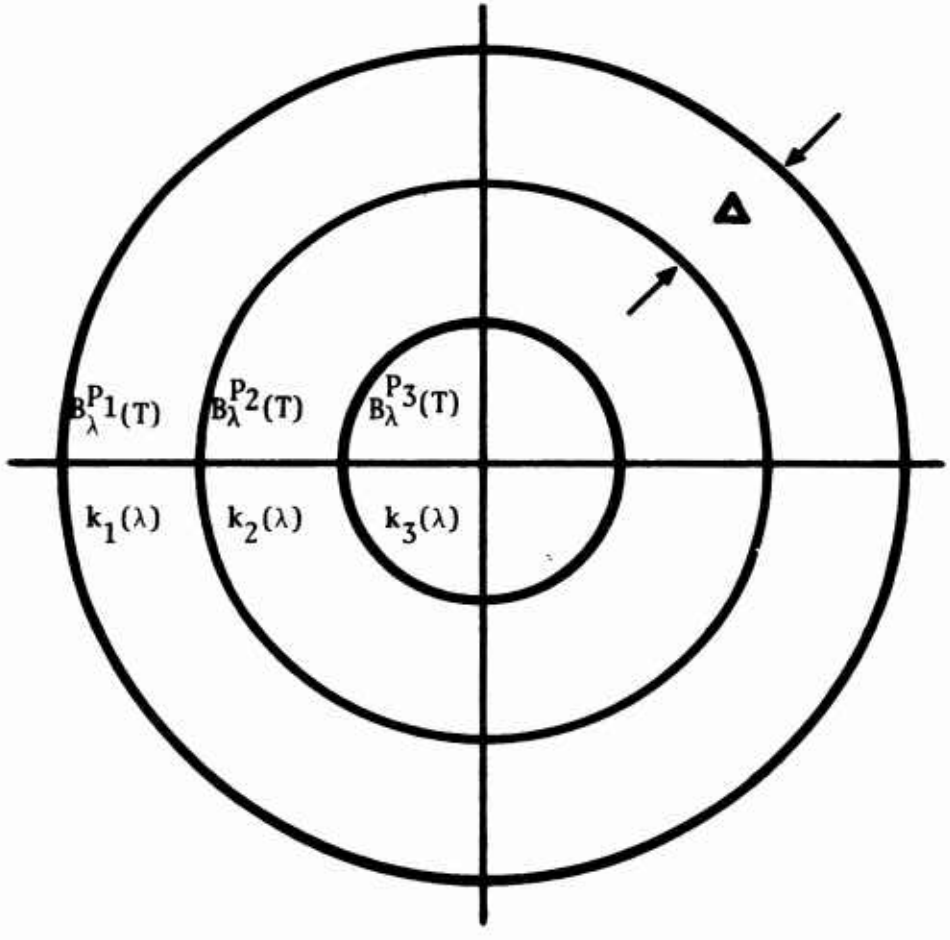

Figure 2. Cross Section of Rocket Produced Plasma Field

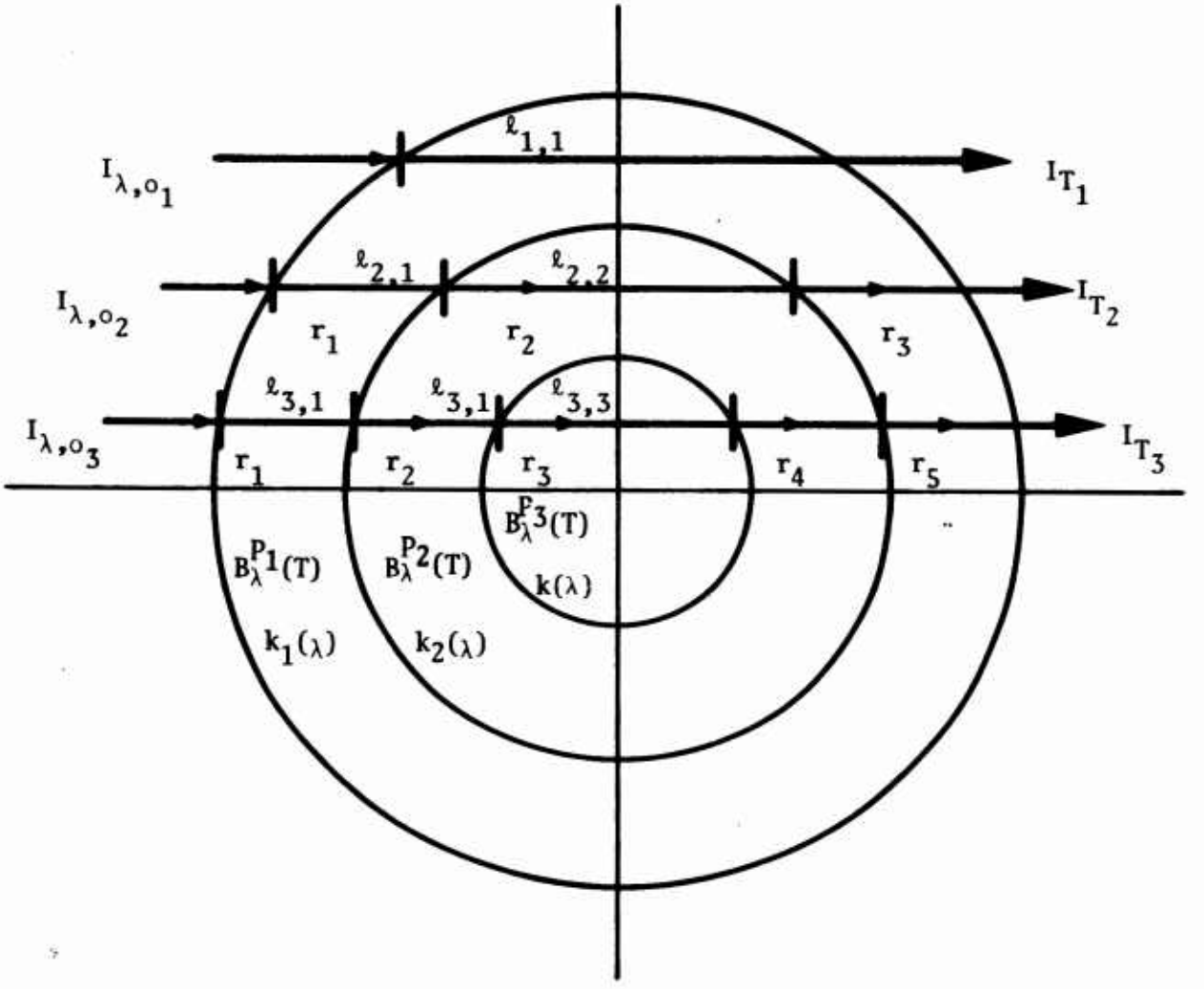

Figure 3. Three Ring Division System

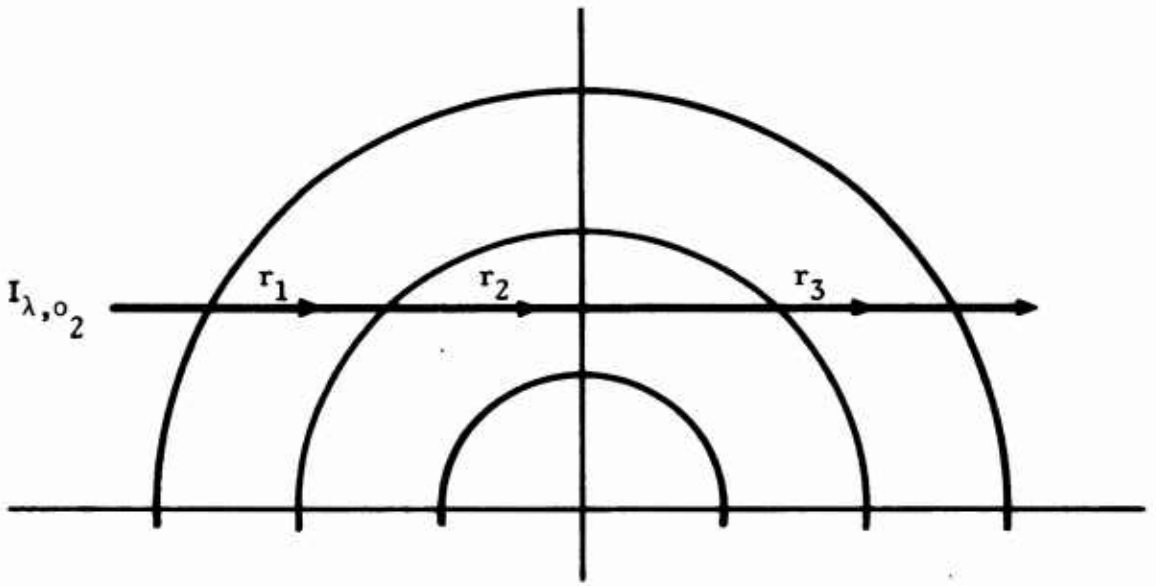

Figure 4. Ray Path Through Two Rings

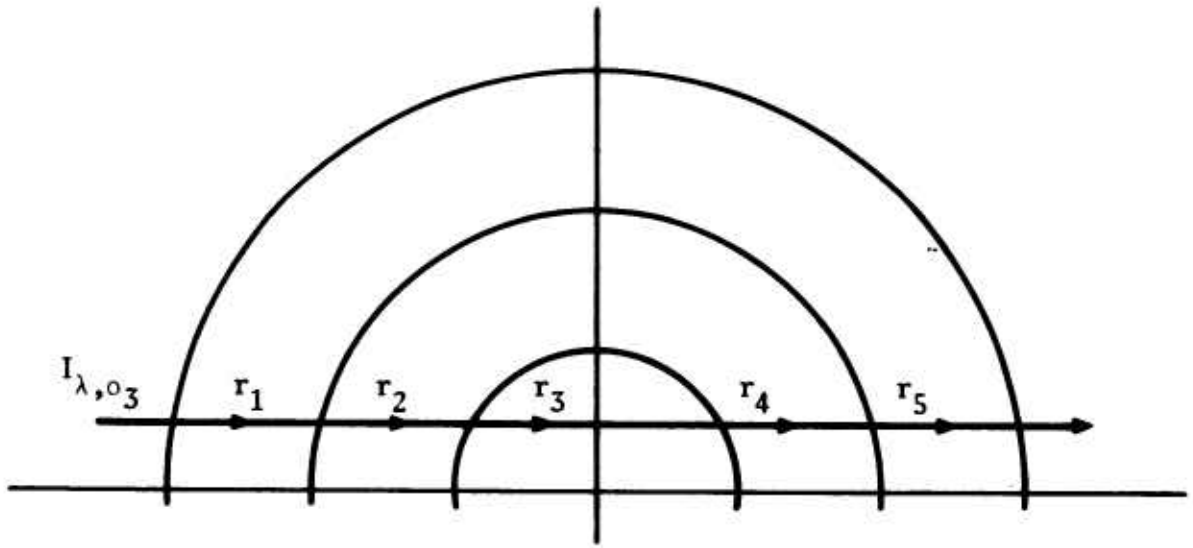

Figure 5. Ray Path Through Three Rings

Experimental Setup for Sodium
Line Reversal Plume Temperature Mapping

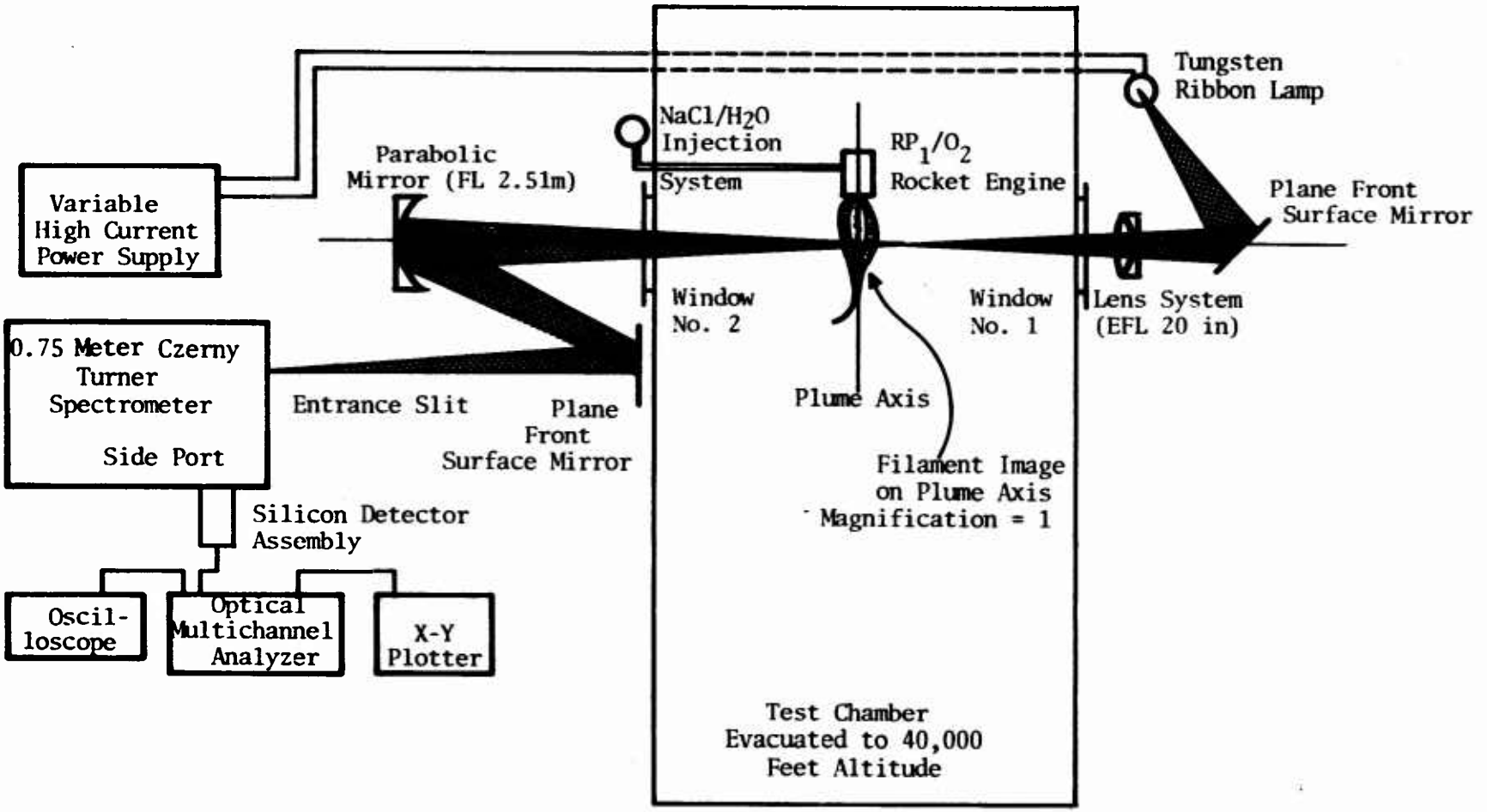

Figure 6. Imaging System

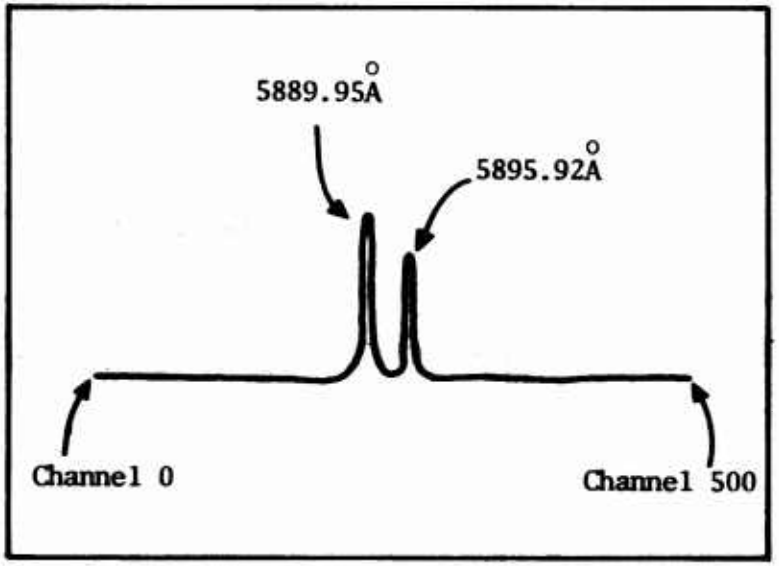

Figure 7. Oscilloscope Display for Sodium Doublet

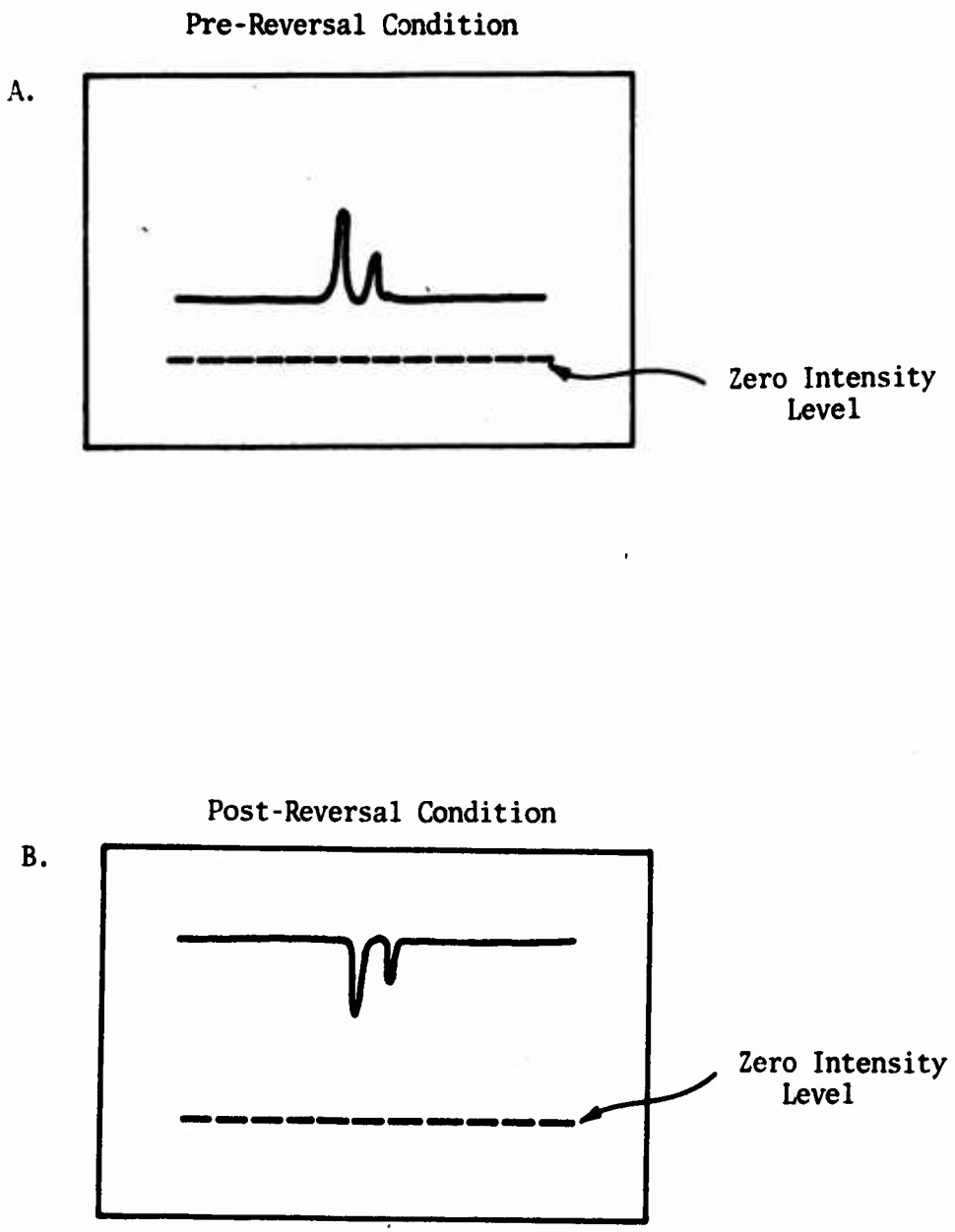

Figure 8. Oscilloscope Displays for Pre- and Post-Reversal

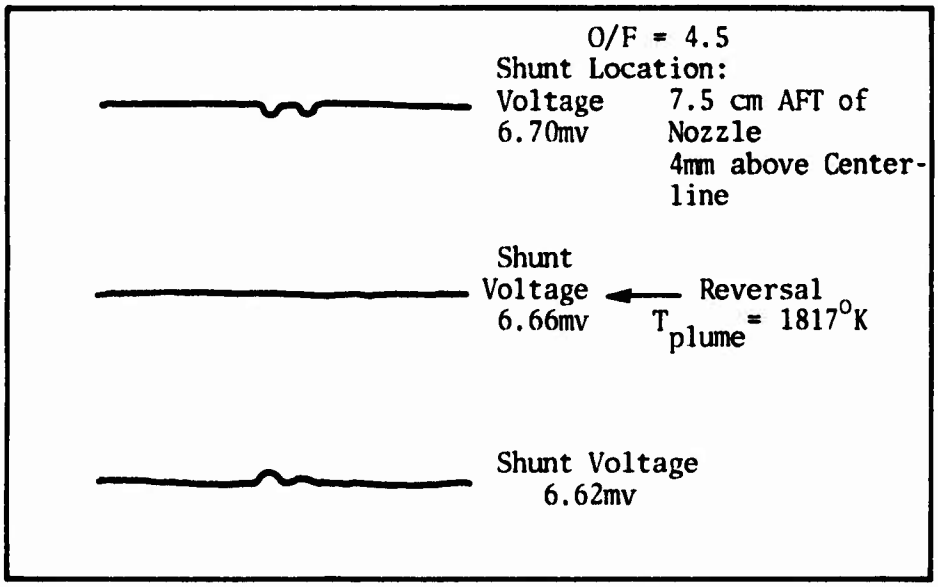

Figure 9. Sample Data Set

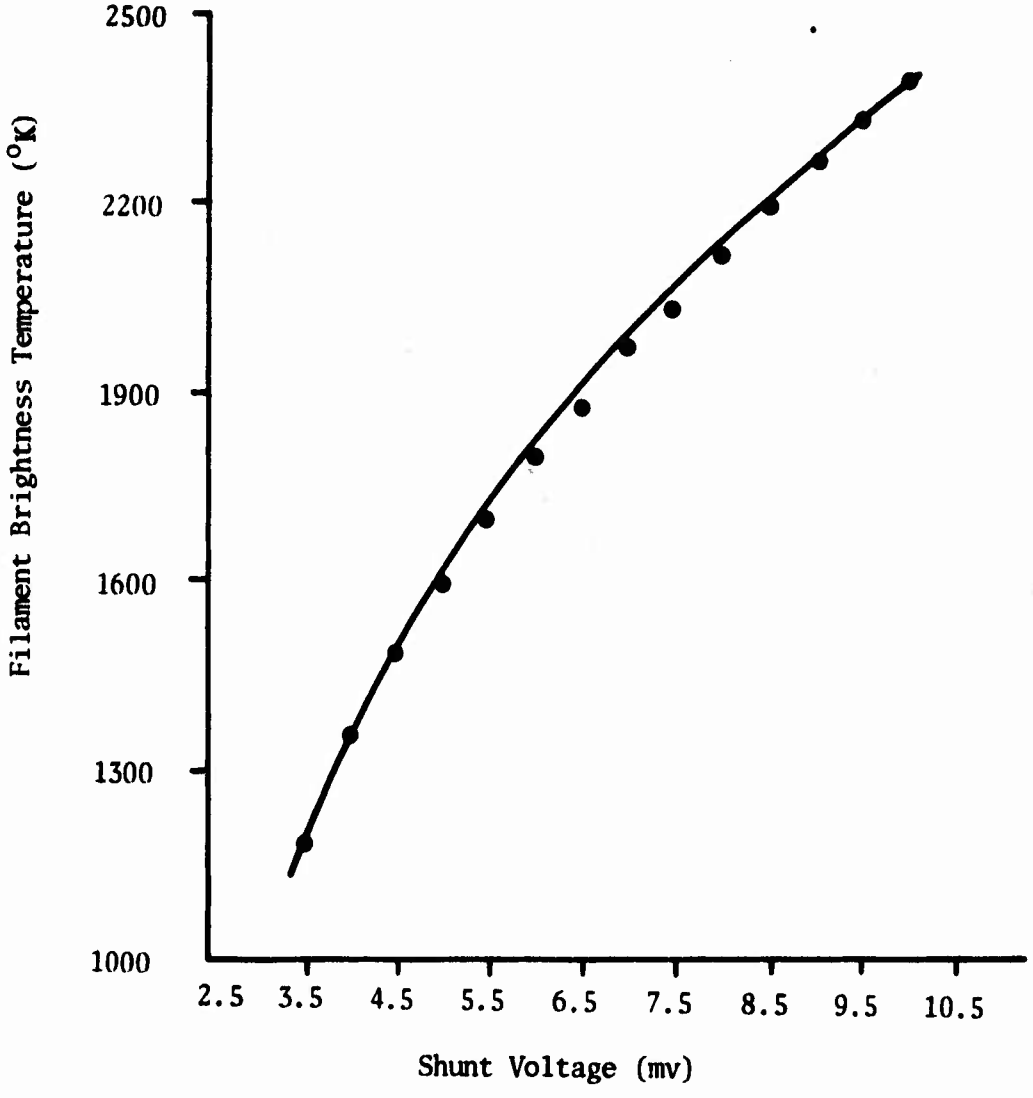

Figure 10. Tungsten Lamp Calibration Curve

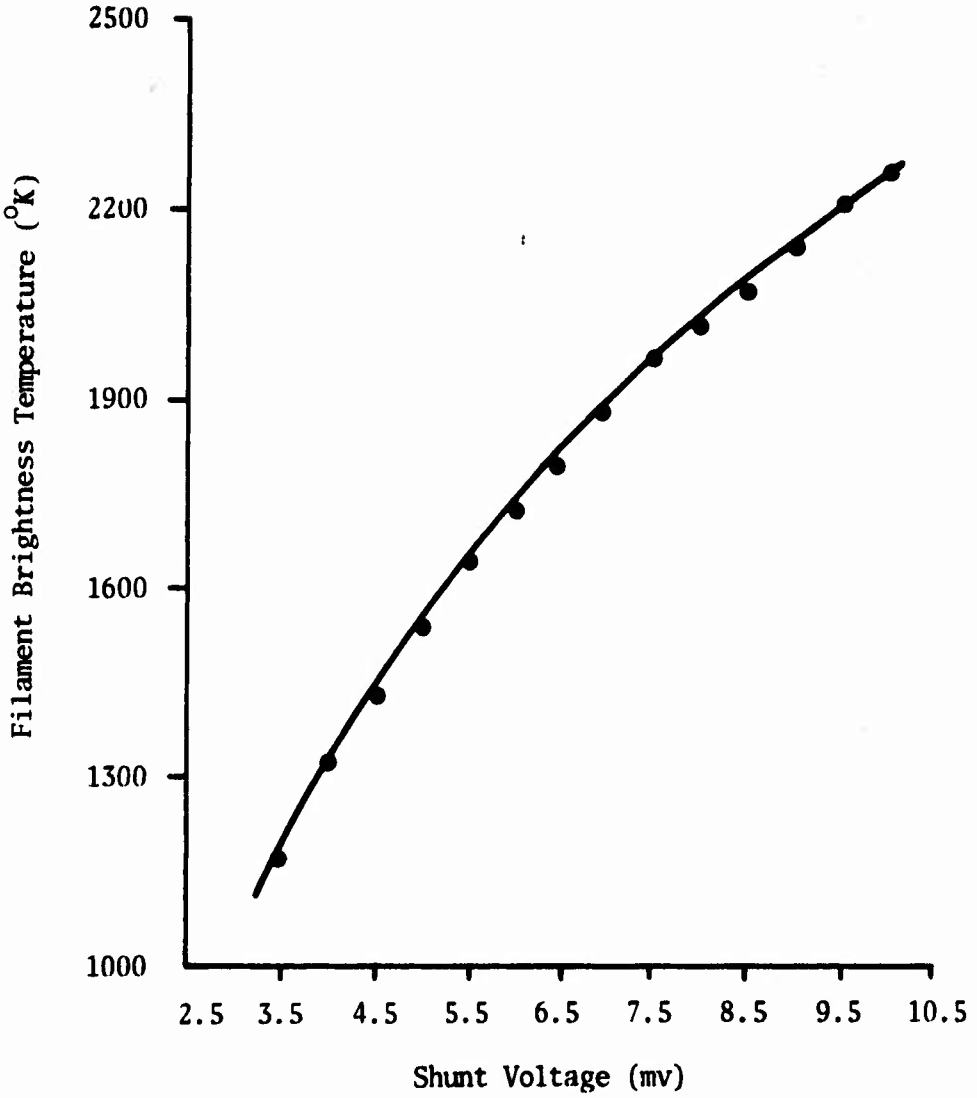

Figure 11. Filament Image Calibration Curve

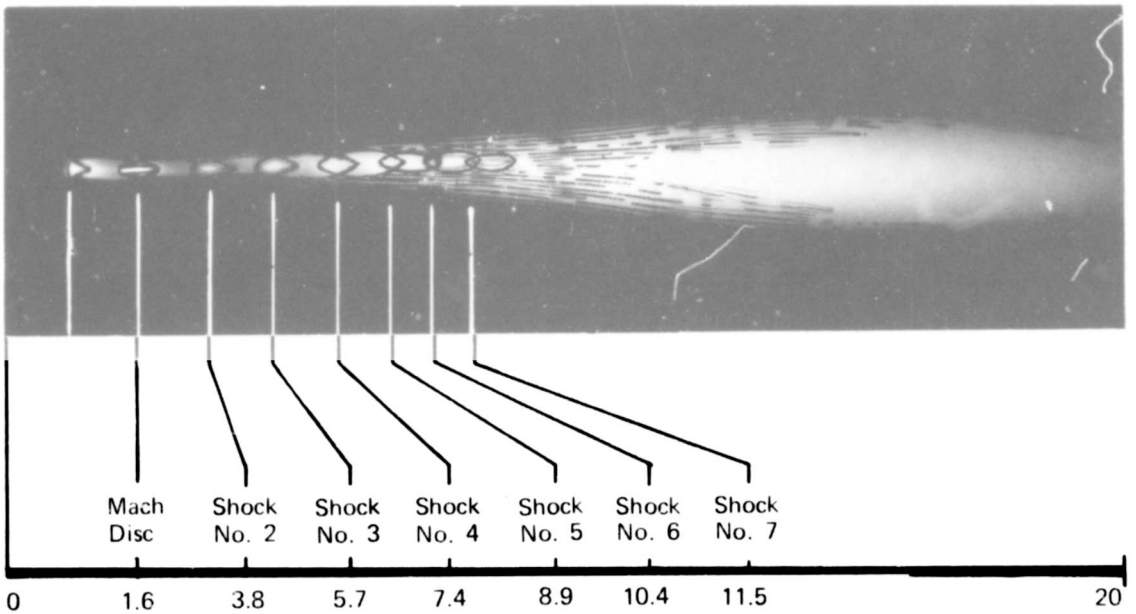

O/F = 2.0

$\dot{m}_t$ = 5 gm/sec

P_c = 4 atm

13.1 km, Static Air

Figure 12. Exhaust Plume

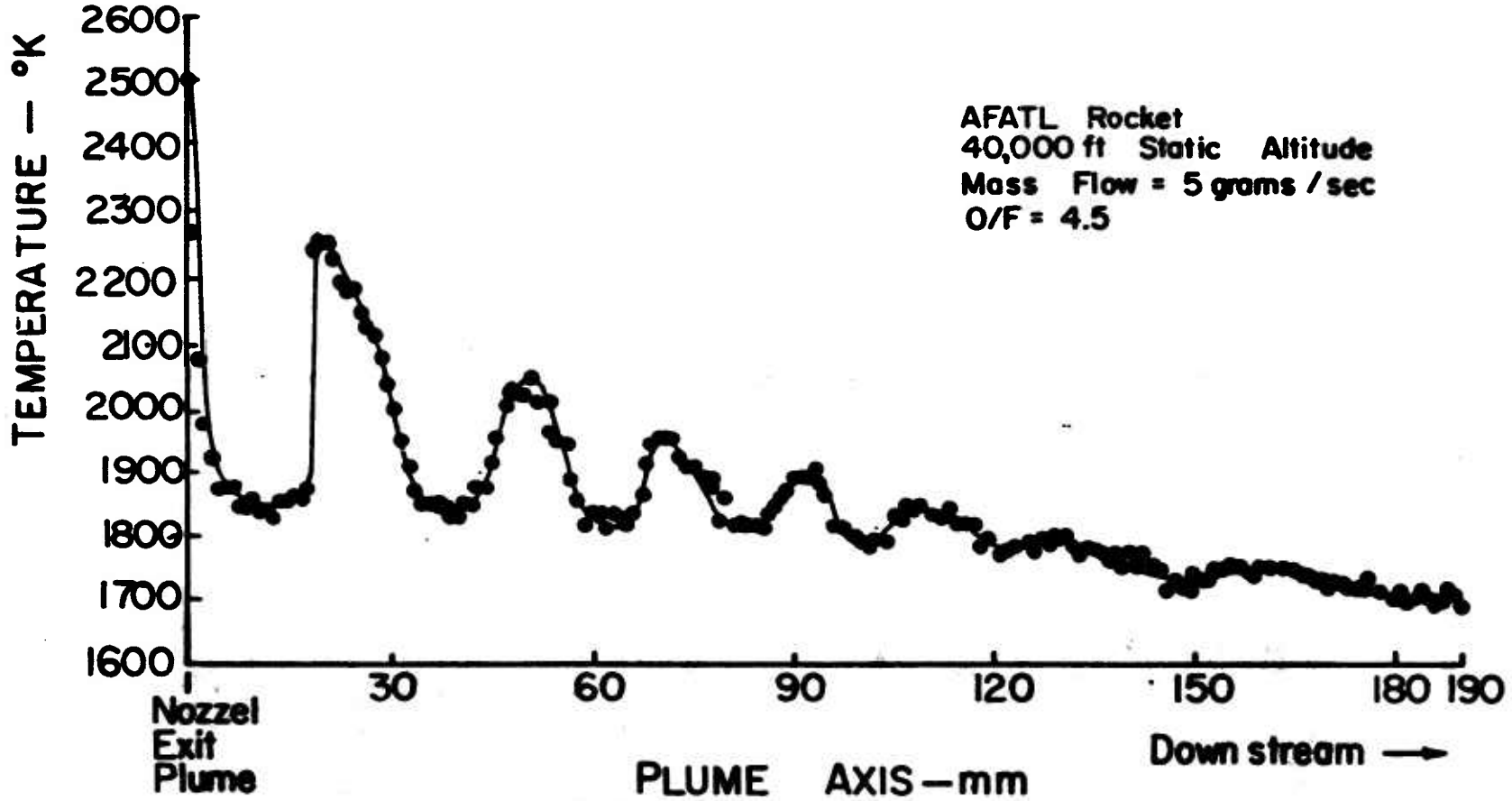

Figure 13. Centerline Temperature Distribution (O/F = 4.5)

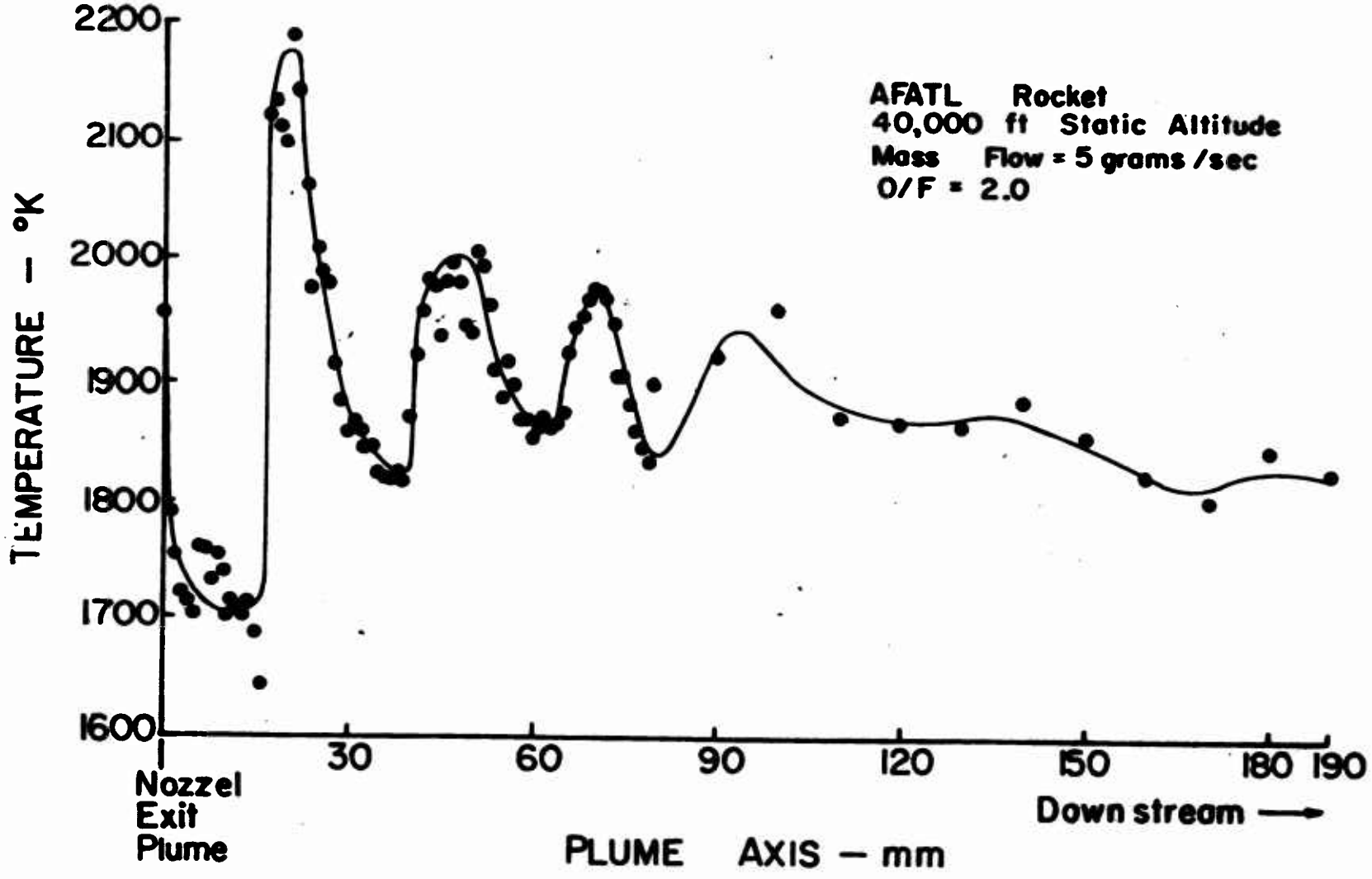

Figure 14. Centerline Temperature Distribution (O/F = 2.0)

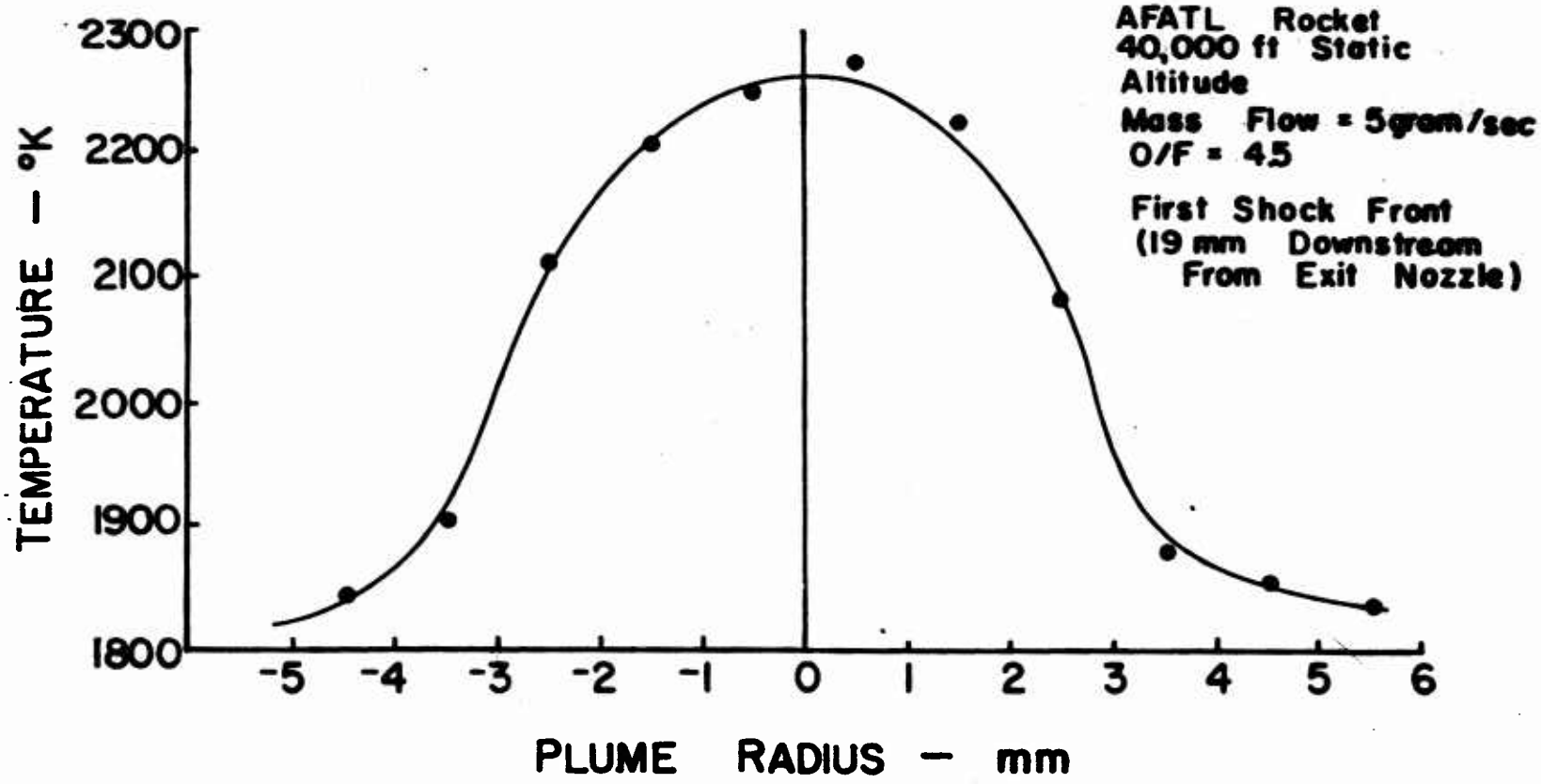

Figure 15. Radial Temperature Distribution (O/F = 4.5)

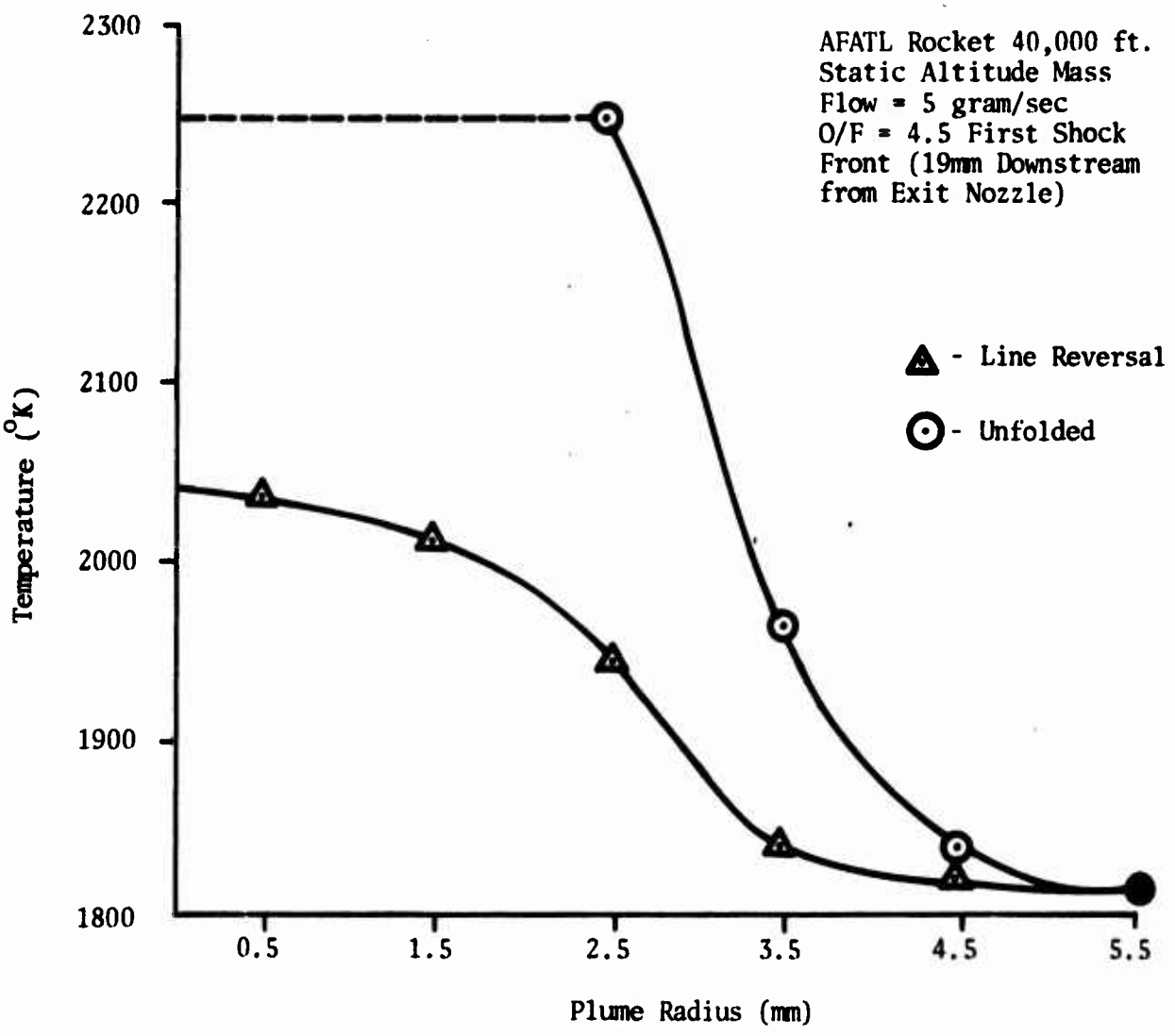

Figure 16. Unfolded Plume Temperature Distribution

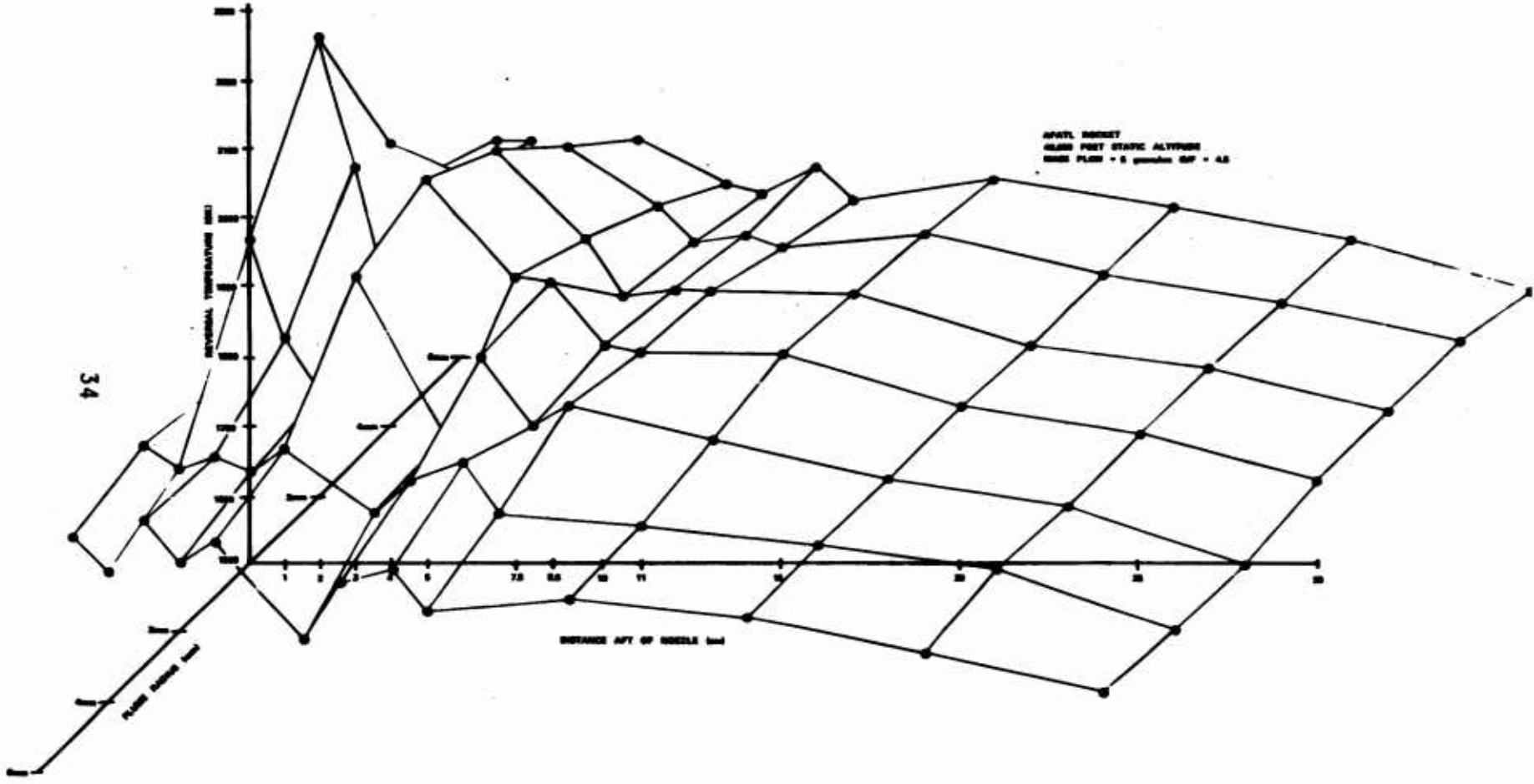

Figure 17. Temperature Map of Plume

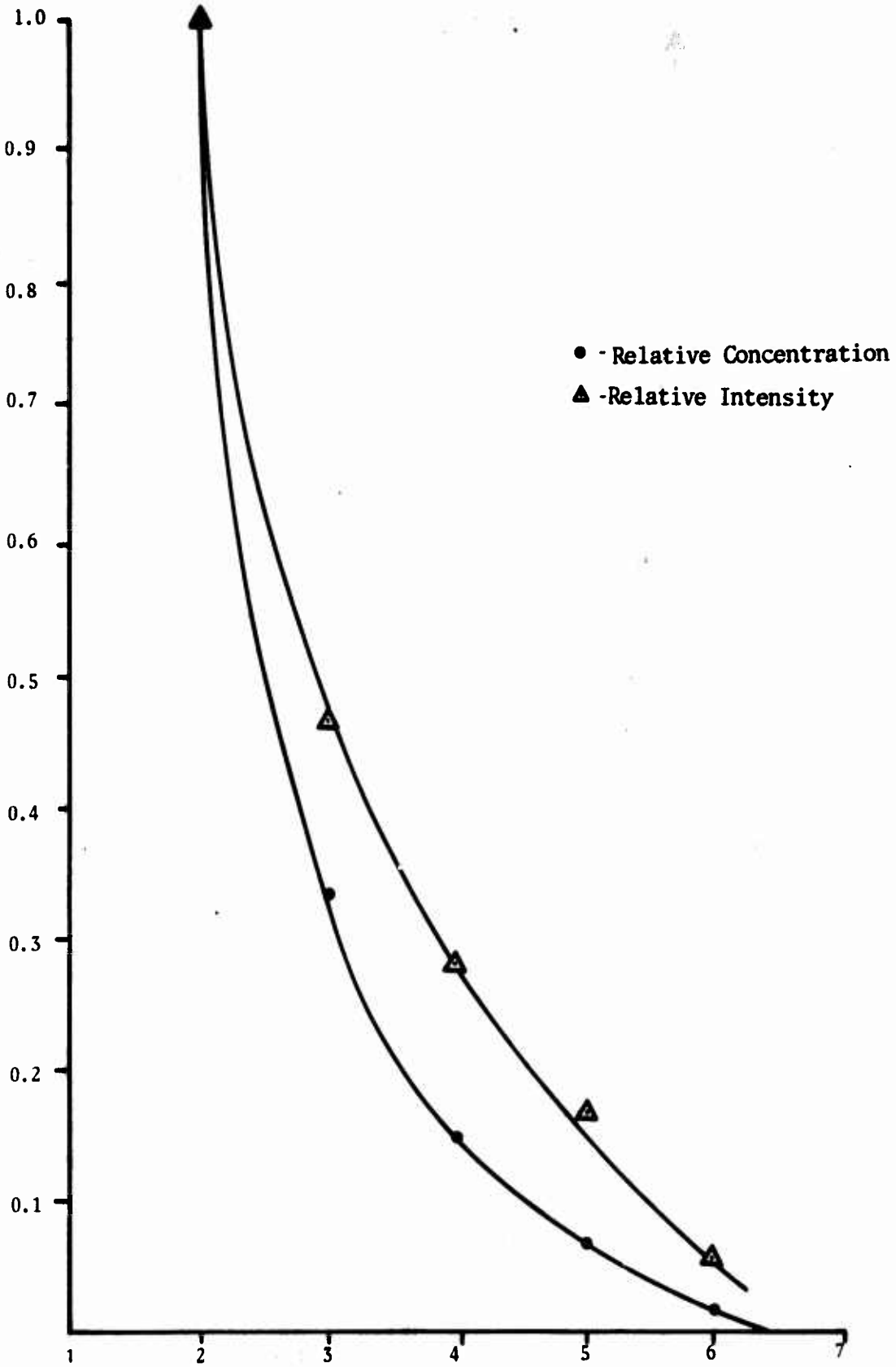

Figure 18. Relative OH Concentration Versus O/F Ratio

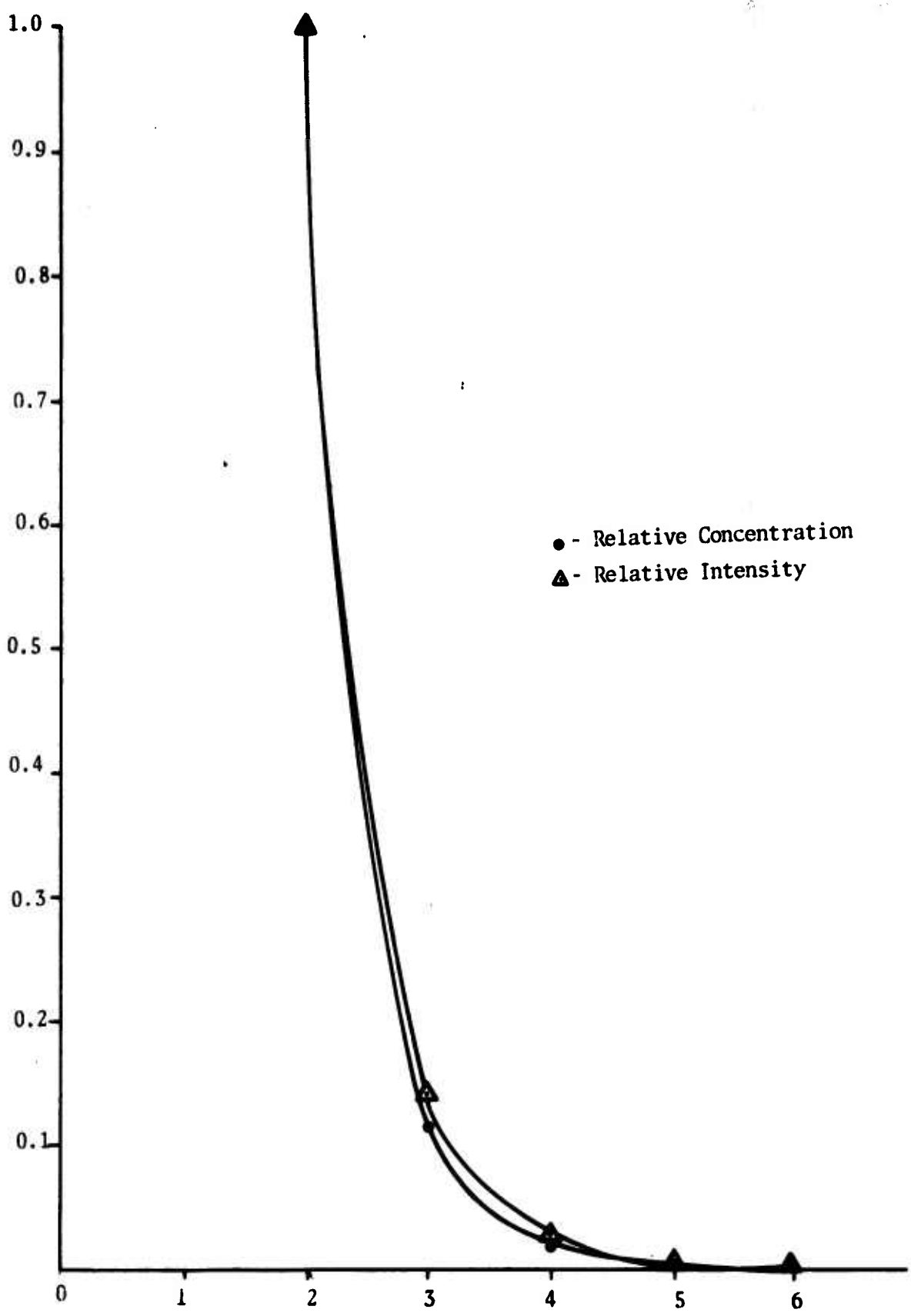

Figure 19. Relative CH Concentration Versus O/F Ratio

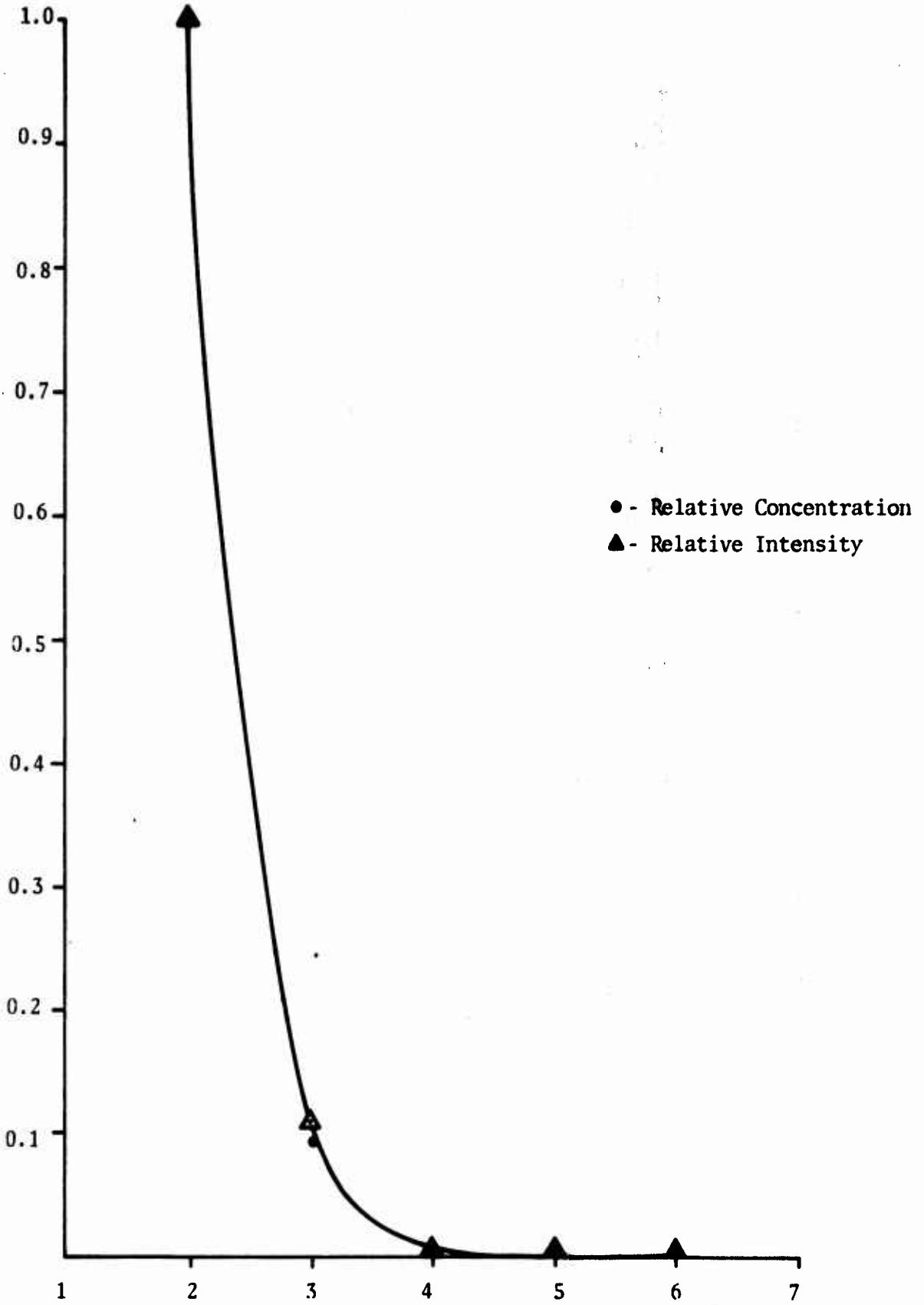

Figure 20. Relative C_2 Concentration Versus O/F Ratio

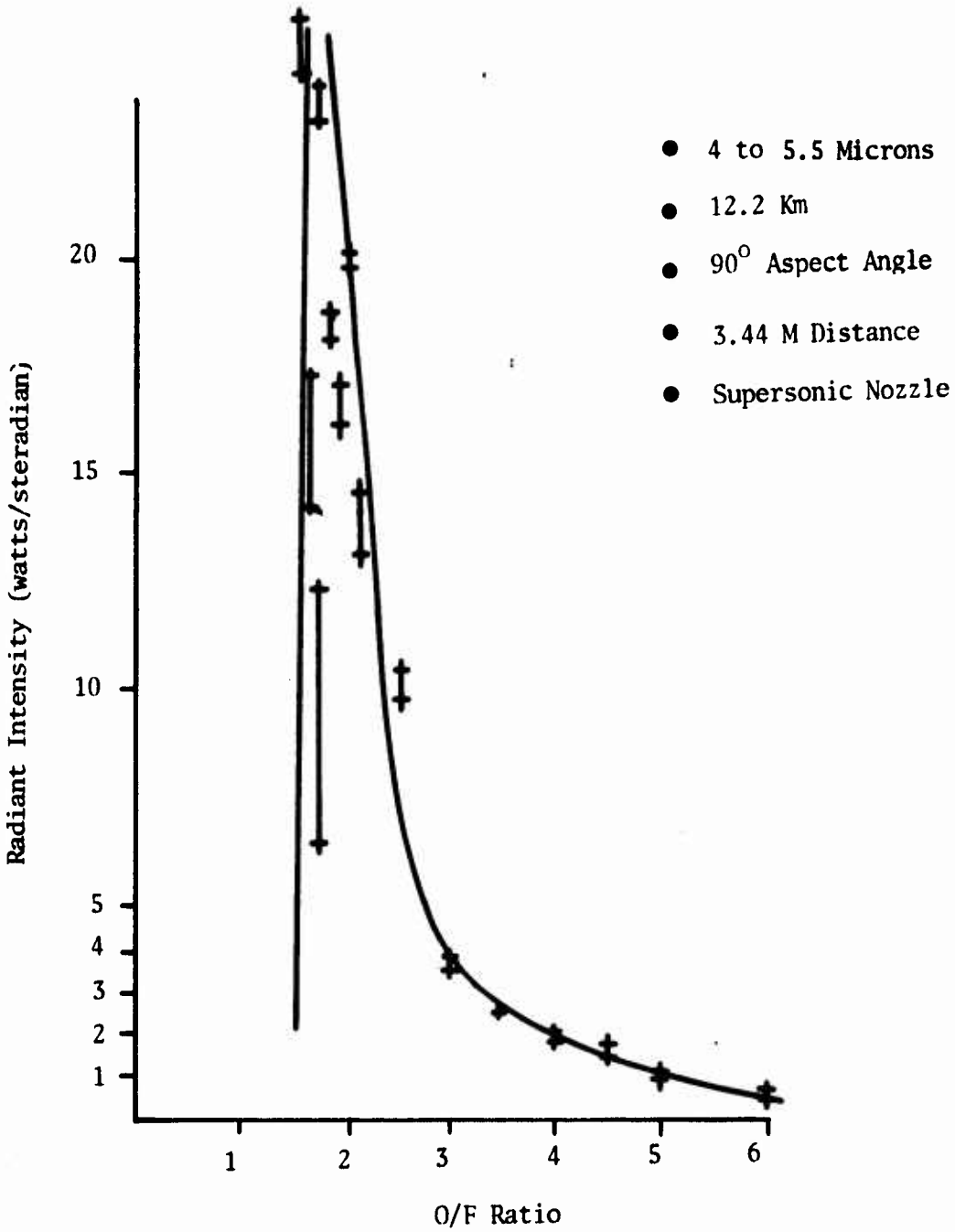

Figure 21. Infrared Radiant Intensity Versus O/F Ratio

REFERENCES

1. J. F. Long, Air Force Armament Laobratory Infrared Plume Simulation Capabilities, Air Force Technical Report No. AFATL-TR-76-26, Air Force Armament Laboratory, Eglin Air Force Base, Florida (May 1976).

2. A. Vamos, Non Equilibrium Effects in Kerosens/O_2 Rocket Nozzle Flows, Technical Report No. AE-75-4, University of Maryland, June 1975.

3. D. B. Ebeoglu and C. W. Martin, Effect of Mixture Ratio on UV. Visible and Infrared Radiation from Exhaust Plumes, Air Force Technical Report No. AFATL-TR-75-79, Air Force Armament Laoboratory, Eglin Air Force Base, Florida, May 1975.

4. G. Herzberg, Molecular Spectra and Molecular Structure, D. Van Nostrand Company, Inc., Toronto, Canada, 1939.

The reverse of this page is blank.

APPENDIX A

DETERMINATION OF SPECIES OF CONCENTRATIONS

CONCENTRATION

For the band-head line of a molecular band we have that

$$I = An^* e^{-E_n/KT}$$

where A is the transition coefficient and E_n is the energy of the upper state. n^* is the density of particles with electrons in energy state E_n. So

$$I = I(n^*T).$$

Then

$$dI = \frac{\partial I}{\partial T}\, dT + \frac{\partial I}{\partial n^*}\, dn^*$$

where $\frac{\partial I}{\partial T} = An^* e^{-E_n/KT} \left(\frac{E_n}{KT^2}\right)$ and

$$\frac{\partial I}{\partial T} - Ae^{-E_n/KT}$$

so $dI = \frac{An^* E_n}{K} \frac{e^{-E_n KT}}{T^2} dt + Ae^{-E_n/KT} dn^*$ and

$$\frac{dI}{I} = \frac{E_N}{K} \frac{dT}{T^2} + \frac{dn^*}{n^*}$$

Integrating

$$\int_{I_{max}}^{I} \frac{dI}{I} + \frac{E_n}{K} \int_{T_{min}}^{T} \frac{dT}{T^2} + \int_{n^*_{max}}^{n} \frac{dn^*}{n^*}$$ and finally

$$\frac{I}{I_{max}} = \exp\left[\frac{E_n}{K}\left(\frac{1}{T_{min}} - \frac{1}{T}\right)\right] \qquad \left(\frac{n^*}{n^*_{max}}\right)$$

$$\text{or } \frac{n^*}{n^*_{max}} = \frac{I}{I_{max}} \left[\exp\left(\frac{-E_n}{K}\right)\left(\frac{1}{T_{min}} - \frac{1}{T}\right)\right]$$

$$\text{Then } n^*_{rel} = I_{rel}\left[\exp\left(\frac{-E_n}{K}\right)\left(\frac{1}{T_{min}} - \frac{1}{T}\right)\right]$$

Thus, the connection between the relative intensity and relative concentration is established.

The relative intensity distribution is obtainable from previous measurements (Reference 3). The E_n are tabulated in the Appendix of Reference 4.

A distribution of the plume temperatures for O/F = 2 through O/F = 6 is obtained by fitting a straight line through two known temperatures. These temperatures were taken to be those measured by sodium line reversal at the first shock front of the plume at the O/F = 2 and O/F = 4.5 conditions.

APPENDIX B

PLUME TEMPERATURE

UNFOLDING TECHNIQUE

UNFOLDING TECHNIQUE

The plume geometry is shown in Figure B-1. The plume cutoff limit was determined photographically to be 7.26 mm from the plume centerline axis. With the exception of the outer ring, all rings have a thickness of 1 mm and data paths are taken through the center of each ring. Poor signal to noise ratio near the outer boundary of the plume prevented the use of a seven-ring system.

All path lengths were determined graphically from a scaled drawing of the plume.

For each path, the following procedure was followed: (1) intensity of the plasma only (I_p) was measured (5889Å) and (2) the tungsten ribbon lamp was increased past the reversal point and the baseline (I_L) and minimum (I_T) intensities were measured. The intensity displays and the tabulated intensities appear in Figure B-2.

A computer program was written in order to simplify the analysis of the data and this appears at the end of this appendix.

The outer ring is taken as ring 1. For data input

$$I_p(n) \rightarrow S(N)$$

$$I_T(n) \rightarrow T(n)$$

$$I_L(n) \rightarrow E(n)$$

The TLAMP (n) value corresponds to the measured line reversal temperatures through each respective path.

The computer output includes a list of the ring absorption coefficients [KAPPA (n)] and the ring temperatures [TEMP (n)].

For the plume data tabulated here the KAPPA (n) are seen to go negative in the fifth and sixth ring. This is caused by the fact that the plasma

is optically very thin ($\kappa \cdot \ell < 1$) and the fact that errors are compounded as the unfolding process advances toward the center ring. Ring temperatures may be obtained only for positive KAPPAS so the generated ring temperatures are useful only through the fourth ring. This indicates that the center temperature of the plume is at least that attained in the fourth ring ($2697^{\circ}K$).

PLUME TEMPERATURE UNFOLDING PROGRAM

```
/list
0000      1 DIMENSION PATH(6,6),KAPPA(6),E(6),T(6),S(6),TERM(6),BPLAS(6),BLAMP
0001       1(6),A(6),V(6),TEMP(6),TLAMP(6)
0002      2 PSUM=0
0003        REAL KAPPA, LAMB, WAVE
0004      3 N=6
0005 $CUTOFF=2
0006      4 D07I=1,N
0007      5 D06J=1
0008      6 PATH(I,J)=0
0009      7 CONTINUE
0010      8 D012I=1,N
0011      9 KAPPA(I)=0
0012     10 E(I)=0
0013     11 T(1)=0
0014     12 CONTINUE
0015     13 MESSAGE'ENTER THE PATH (I,J) VALUES'
0016     14 DO20I=1,N
0017     15 DO19J=1,I
0018     16 MESSAGE'PATH SUB'
0019     17 WRITE(6)I,J
0020     18 MESSAGE'EQUALS'
0021     19 READ(5)PATH(I,J)
0022     20 CONTINUE
0023     21 MESSAGE'ENTER THE E(N) VALUES'
0024     22 DO26I=1,N
0025     23 MESSAGE'E SUB'
0026     24 WRITE(6)I,J
0027     25 MESSAGE'EQUALS
0028     26 READ(5)E(I)
0029     27 MESSAGE'ENTER THE T(N) VALUES'
0030     28 DO32I=1,N
0031     29 MESSAGE'T SUB'
0032     30 WRITE(6)I
0033     31 MESSAGE'EQUALS'
```

```
0034     32 READ(5)T(I)
0035     33 MESSAGE'ENTER THE S(N) VALUES'
0036     34 D038I=1,N
0037     35 MESSAGE'S SUB'
0038     36 WRITE(6)I
0039     37 MESSAGE'EQUALS'
0040     38 READ(5)S(I)
0041     39 D045I=1,N
0042     40 TERM(I)=(ALOG(E(I)/(T(I)-S(I))))/(2*PATH(I,I))
0043     41 D043J=1,I-1
0044     42 PSUM=PSUM+(KAPPA(J)*PATH(I,J))
0045     43 CONTINUE
0046     44 KAPPA(I)=TERM(I)-(PSUM/PATH(I,I))
0047     45 PSUM=0
0048     46 MESSAGE' THE KAPPA VALUES APPEAR BELOW'
0049     47 D051I=1,N
0050     48 MESSAGE'KAPPA SUB'
0051     49 WRITE(6)I
0052     50 MESSAGE'EQUALS'
0053     51 WRITE(6)KAPPA(I)
0054     52 D058J=1,N
0055     53 BPLAS(J)=0
0056     54 BLAMP(J)=0
0057     55 A(J)=0
0058     56 V(J)=0
0059     57 TEMP(J)=0
0060     58 CONTINUE
0061     59 MESSAGE 'ENTER LAMBDA DESIRED IN ANGSTROMS'
0062     60 READ(5)LAMB
0063     61 MESSAGE 'ENTER TEMPERATURE OF OUTER RING IN DEGREES KELVIN'
0064     62 READ(5)TEMP(1)
0065     63 MESSAGE 'ENTER THE TLAMP VALUES'
0066     64 D069J=1,N
0067     65 MESSAGE'TLAMP SUB'
0068     66 WRITE(6) J
0069     67 MESSAGE'EQUALS'
0070     68 READ(5)TLAMP(J)
```

```
0071      69 CONTINUE
0072      70 D073J=1,N
0073      71 WAVE=(LAMB)*(1.E-8)
0074      72 BLAMP(J)=(1.191E-5)*(WAVE**-5)/(EXP(1.4388/WAVE/TLAMP(J)))
0075      73 CONTINUE
0076      74 BPLAS(1)=BLAMP(1)
0077      75 D085I=2,N
0078      76 A(1)=BPLAS(1)*(1-EXP((-1)*(KAPPA(1))*(PATH(I,1))))+BLAMP(I)*(EXP((
0079        1-1)*(KAPPA(1))*(PATH(I,1))))
0080      77 D079J=2,I-1
0081      78 A(J)=BPLAS(J)*(1-EXP((-1)*(KAPPA(J))*(PATH(I,J))))+A(J-1)*(EXP((-1
0082        1)*(KAPPA(J))*(PATH(I,J))))
0083      79 CONTINUE
0084      80 V(1)=(BLAMP(I)-((BPLAS(1))*(1-EXP((-1)*(KAPPA(1))*(PATH(I,1))))))/
0085        1(EXP((-1)*(KAPPA(1))*(PATH(I,1))))
0086      81 D083J=2,I-1
0087      82 V(J)=(V(J-1)-((BPLAS(J))*(1-EXP((-1)*(KAPPA(J))*(PATH(I,J))))))/(E
0088        1XP((-1)*(KAPPA(J))*(PATH(I,J))))
0089      83 CONTINUE
0090      84 BPLAS(I)=(V(I-1)-(A(I-1)*(EXP((-2)*(KAPPA(I))*(PATH(I,I))))))/(1-E
0091        1XP((-2)*(KAPPA(I))*(PATH(I,I))))
0092      85 CONTINUE
0093      86 D088J=1,N
0094         WAVE=LAMB*1.E-8
0095      87 TEMP(J)+(1.4388/WAVE(*(1/ALOG(((1.19E-5)*(WAVE**-5)/BPLAS(J))+1))
0096      88 CONTINUE
0097      89 D094J=1,N
0098      90 MESSAGE 'TEMP SUB'
0099      91 WRITE(6)J
0100      92 MESSAGE'EQUALS'
0101      93 WRITE(6)TEMP(J)
0102      94 CONTINUE
0103      95 END
END OF WORK FILE
```

DATA INPUT (PATH VALUES)

```
BEGIN COMPILATION      134
ENTER THE PATH (I,J) VALUES
PATH SUB
I= 1 J= 1
EQUALS
021     19 READ(5)PATH(I,J)
.483
PATH SUB
I= 2 J= 1
EQUALS
021     19 READ(5)PATH(I,J)
.352
PATH SUB
I= 2 J= 2
EQUALS
021     19 READ(5)PATH(I,J)
.215
PATH SUB
I= 3 J= 1
EQUALS
021     19 READ(5)PATH(I,J)
.280
PATH SUB
I= 3 J= 2
EQUALS
021     19 READ(5)PATH(I,J)
.165
PATH SUB
I= 3 J= 3
EQUALS
021     19 READ(5)PATH(I,J)
.192
PATH SUB
I= 4 J= 1
EQUALS
021     19 READ(5)PATH(I,J)
.248
PATH SUB
I= 4 J= 2
EQUALS
021     19 READ(5)PATH(I,J)
.123
PATH SUB
I= 4 J= 3
EQUALS
021     19 READ(5)PATH(I,J)
.146
PATH SUB
I= 4 J= 4
EQUALS
021     19 READ(5)PATH(I,J)
.164
PATH SUB
I= 5 J= 1
EQUALS
021     19 READ(5)PATH(I,J)
.233
PATH SUB
I= 5 J= 2
EQUALS
021     19 READ (5) PATH(I,J)
.106
PATH SUB
I= 5 J= 3
EQUALS
021     19 READ(5)PATH(I,J)
.111
PATH SUB
I= 5 J= 4
EQUALS
021     19 READ(5)PATH(I,J)
.128
PATH SUB
I= 5 J= 5
EQUALS
021     19 READ(5)PATH(I,J)
.130
PATH SUB
I= 6 J= 1
EQUALS
021     19 READ(5)PATH(I,J)
.226
PATH SUB
I= 6 J= 2
EQUALS
021     19 READ(5)PATH(I,J)
.103
PATH SUB
I= 6 J= 3
EQUALS
021     19 READ(5)PATH(I,J)
.102
PATH SUB
I= 6 J= 4
EQUALS
021     19 READ(5)PATH(I,J)
.102
PATH SUB
I= 6 J= 5
EQUALS
021     19 READ(5)PATH(I,J)
.106
PATH SUB
I= 6 J= 6
EQUALS
021     19 READ(5)PATH(I,J)
.086
ENTER THE E(N) VALUES
E SUB
I= 1
EQUALS
028     26 READ(5)E(I)
195
```

INPUT (LINE REVERSAL TEMPERATURES)

```
ENTER LAMBDA DESIRED IN ANGSTROMS
038     60 READ(5)LAMB
5889.95
ENTER TEMPERATURE OF OUTER RING IN DEGREES DELVIN
040     62 READ(5)TEMP(1)
1833
ENTER THE TLAMP VALUES
TLAMP SUB
J= 1
EQUALS
046     68 READ(5)TLAMP(J)
1833
TLAMP SUB
J= 2
EQUALS
046     68 READ(5)TLAMP(J)
1852
TLAMP SUB
J= 3
EQUALS
046     68 READ(5)TLAMP(J)
1877
TLAMP SUB
J= 5
EQUALS
046     68 READ(5)TLAMP(J)
2222
TLAMP SUB
J= 6
EQUALS
046     68 READ(5)TLAMP(J)
2272
```

OUTPUT (KAPPA VALUES)

```
 THE KAPPA VALUES APPEAR BELOW
KAPPA SUB
I= 1
EQUALS
KAPPA(1)= 0.485485
KAPPA SUB
I= 2
EQUALS
KAPPA(2)= 0.607077
KAPPA SUB
I= 3
EQUALS
KAPPA(3)= 0.561228E-01
KAPPA SUB
I= 4
EQUALS
KAPPA(4)= 0.6684593-01
KAPPA SUB
I= 5
EQUALS
KAPPA(5)= -0.964486
KAPPA SUB
I= 6
EQUALS
KAPPA(6)= -0.326086
```

DATA INPUT (INTENSITY VALUES)

```
E SUB
I= 2
EQUALS
028       26 READ(5)E(I)
201
E SUB
I= 3
EQUALS
028       26 READ(5)E(I)
213
E SUB
I= 4
EQUALS
028       26 READ(5)E(I)
396
E SUB
I= 5
EQUALS
028       26 READ(5)E(I)
679
E SUB
I= 6
EQUALS
028       26 READ(5)E(I)
881
ENTER THE T(N) VALUES
T SUB
I= 1
EQUALS
034       32 READ(5)T(I)
139
T SUB
I= 2
EQUALS
034       32 READ(5)T(I)
127
T SUB
I= 3
EQUALS
034       32 READ(5)T(I)
153
T SUB
I= 4
EQUALS
034       32 READ(5)T(I)
310
T SUB
I= 5
EQUALS
034       32 READ(5)T(I)
660
T SUB
I= 6
EQUALS
034       32 READ(5)T(I)
860
ENTER THE S(N) VALUES
S SUB
I= 1
EQUALS
040       38 READ(5)S(I)
17
S SUB
I= 2
EQUALS
040       38 READ(5)S(I)
17
S SUB
I= 3
EQUALS
040       38 READ(5)S(I)
23
S SUB
I= 4
EQUALS
040       38 READ(5)S(I)
52
S SUB
I= 5
EQUALS
040       38 READ(5)S(I)
66
S SUB
I= 6
EQUALS
040       38 READ(5)S(I)
70
```

OUTPUT (RING TEMPERATURES)

```
TEMP SUB
J= 1
EQUALS
TEMP(1)= 1833.11
TEMP SUB
J= 2
EQUALS
TEMP(2)= 1874.55
TEMP SUB
J= 3
EQUALS
TEMP(3)= 2126.75
TEMP SUB
J= 4
EQUALS
TEMP(4)= 2696.90
```

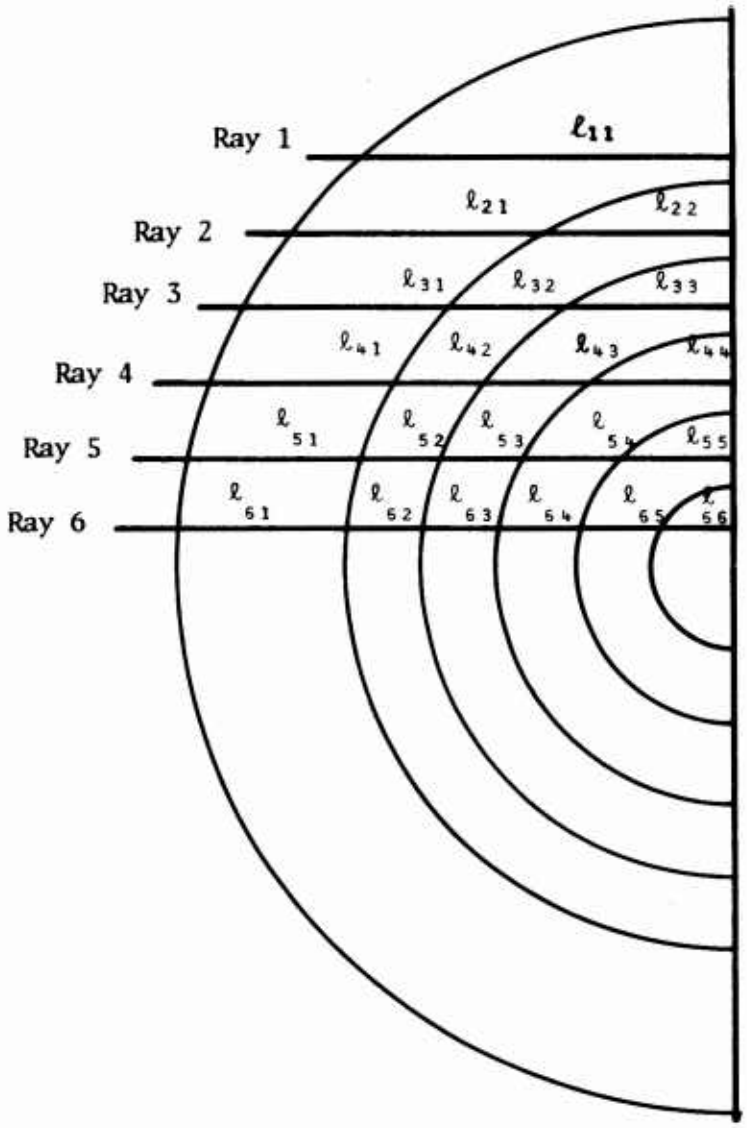

ℓ_{11} = 4.83mm

ℓ_{21} = 3.52mm ℓ_{22} = 2.15mm

ℓ_{31} = 2.80mm ℓ_{32} = 1.65mm ℓ_{33} = 1.92mm

ℓ_{41} = 2.48mm ℓ_{42} = 1.23mm ℓ_{43} = 1.46 ℓ_{44} = 1.64mm

ℓ_{51} = 2.33mm ℓ_{52} = 1.06mm ℓ_{53} = 1.11mm ℓ_{54} = 1.28mm
ℓ_{55} = 1.30mm

ℓ_{61} = 2.26mm ℓ_{62} = 1.03mm ℓ_{63} = 1.02mm ℓ_{64} = 1.02mm
ℓ_{65} = 1.06mm ℓ_{66} = .86mm

Figure B-1. Plume Geometry

All Intensities in Relative Units

$I_p(1) = 17$
$I_p(2) = 17$
$I_p(3) = 23$
$I_p(4) = 52$
$I_p(5) = 66$
$I_p(6) = 70$

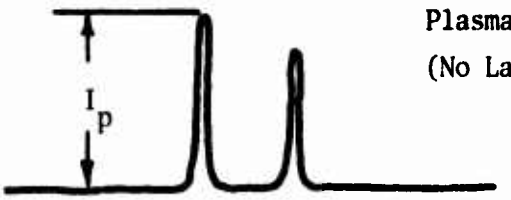

Plasma Only
(No Lamp)

$I_L(1) = 195$ $I_T(1) = 139$
$I_L(2) = 201$ $I_T(2) = 127$
$I_L(3) = 213$ $I_T(3) = 153$
$I_L(4) = 396$ $I_T(4) = 310$
$I_L(5) = 679$ $I_T(5) = 660$
$I_L(6) = 881$ $I_T(6) = 860$

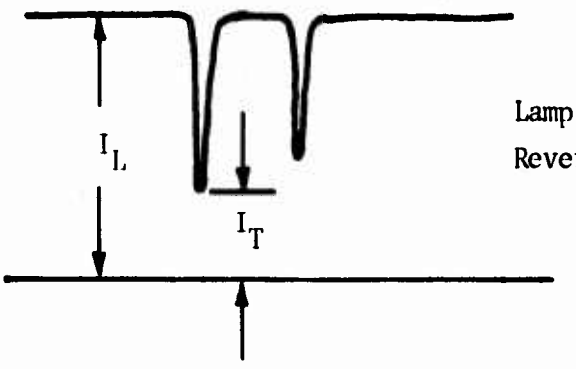

Lamp Driven Past
Reversal Point

Figure B-2. Data Collection Technique

APPENDIX C

RADIAL TEMPERATURE SCANS

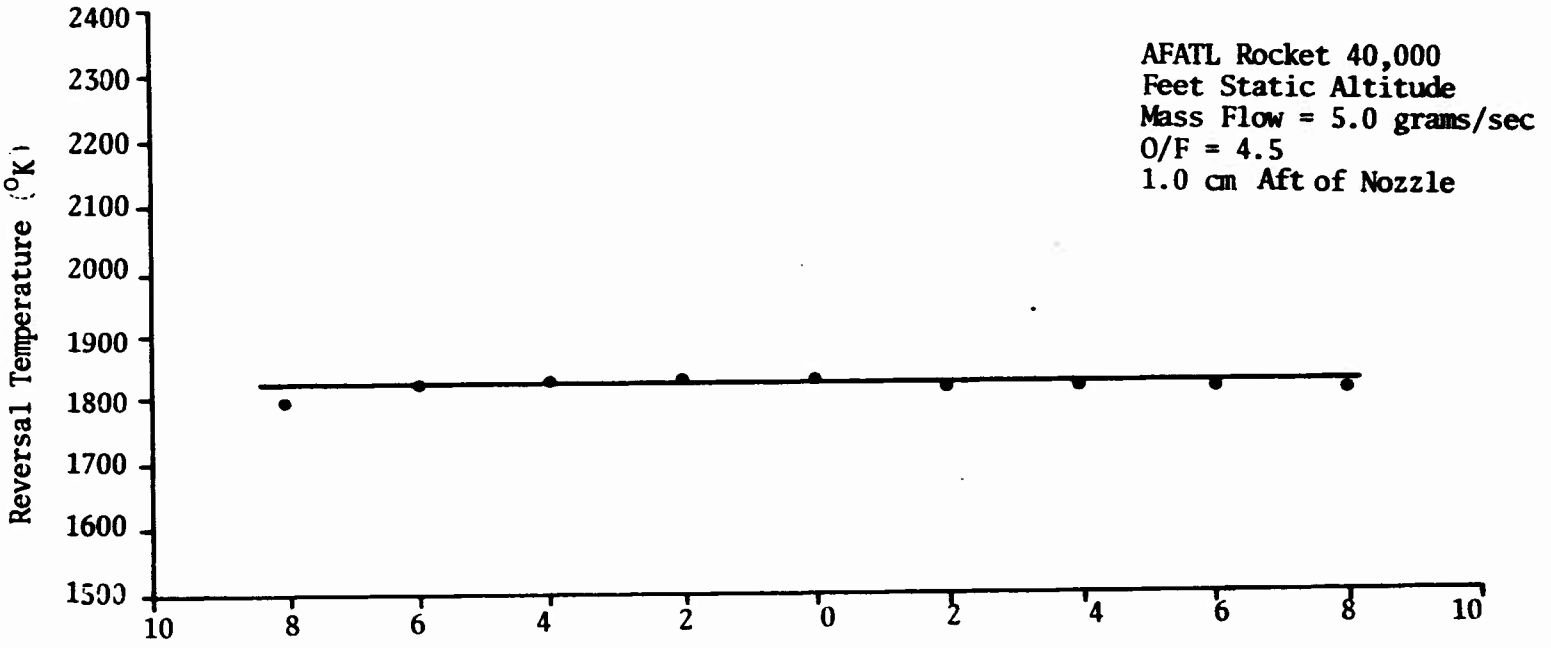

Figure C-1. Radial Temperature Scan (1.0 cm Aft of Rocket Nozzle)

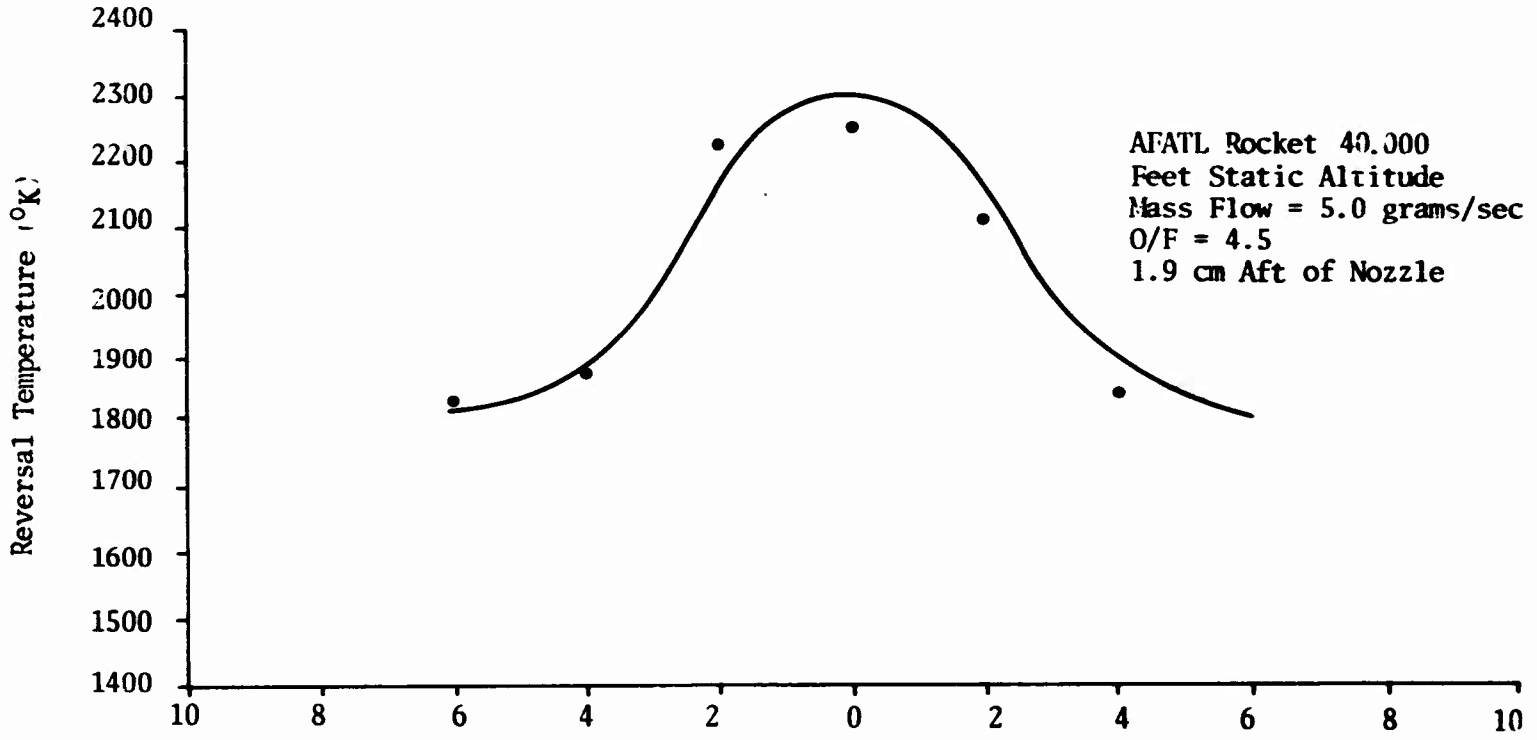

Figure C-2. Radial Temperature Scan (1.9 cm Aft of Rocket Nozzle)

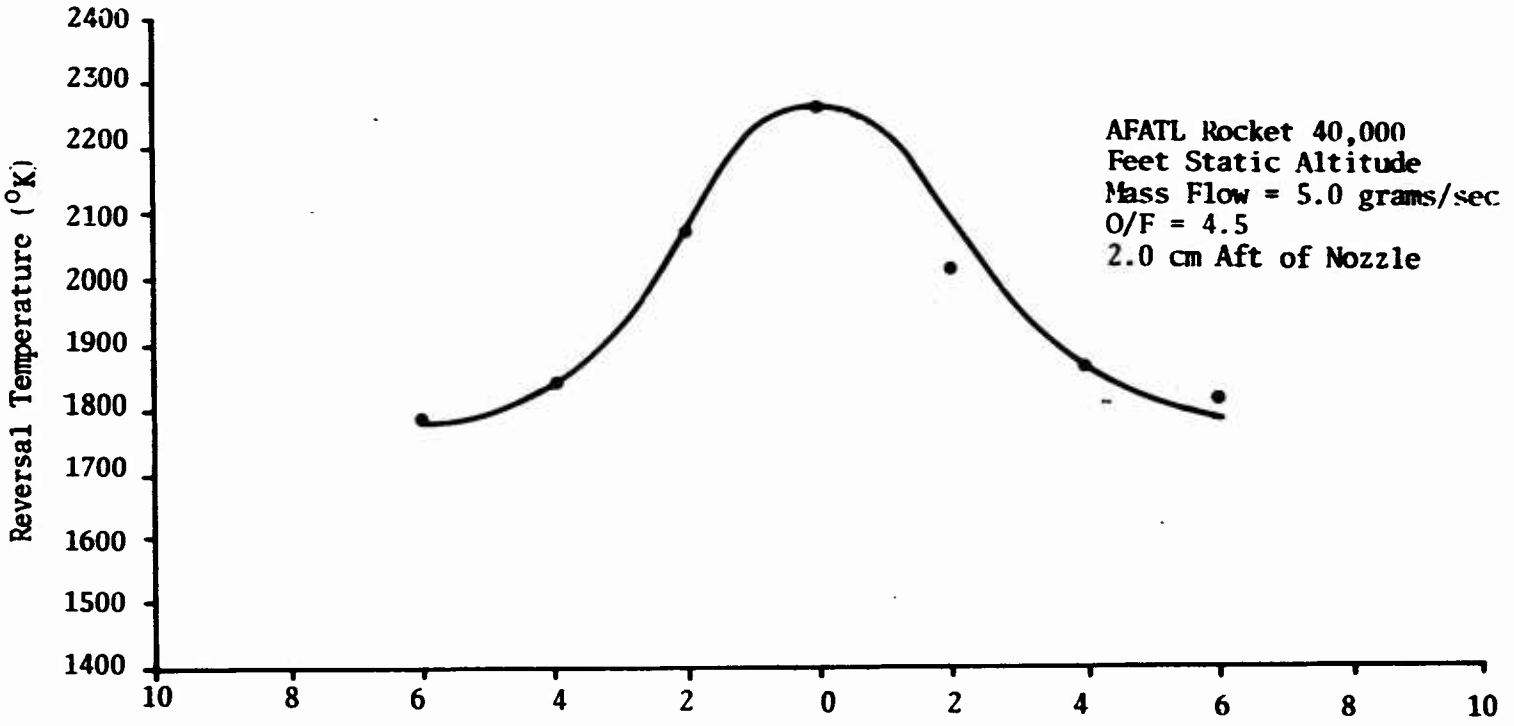

Figure C-3. Radial Temperature Scan (2.0 cm Aft of Rocket Nozzle)

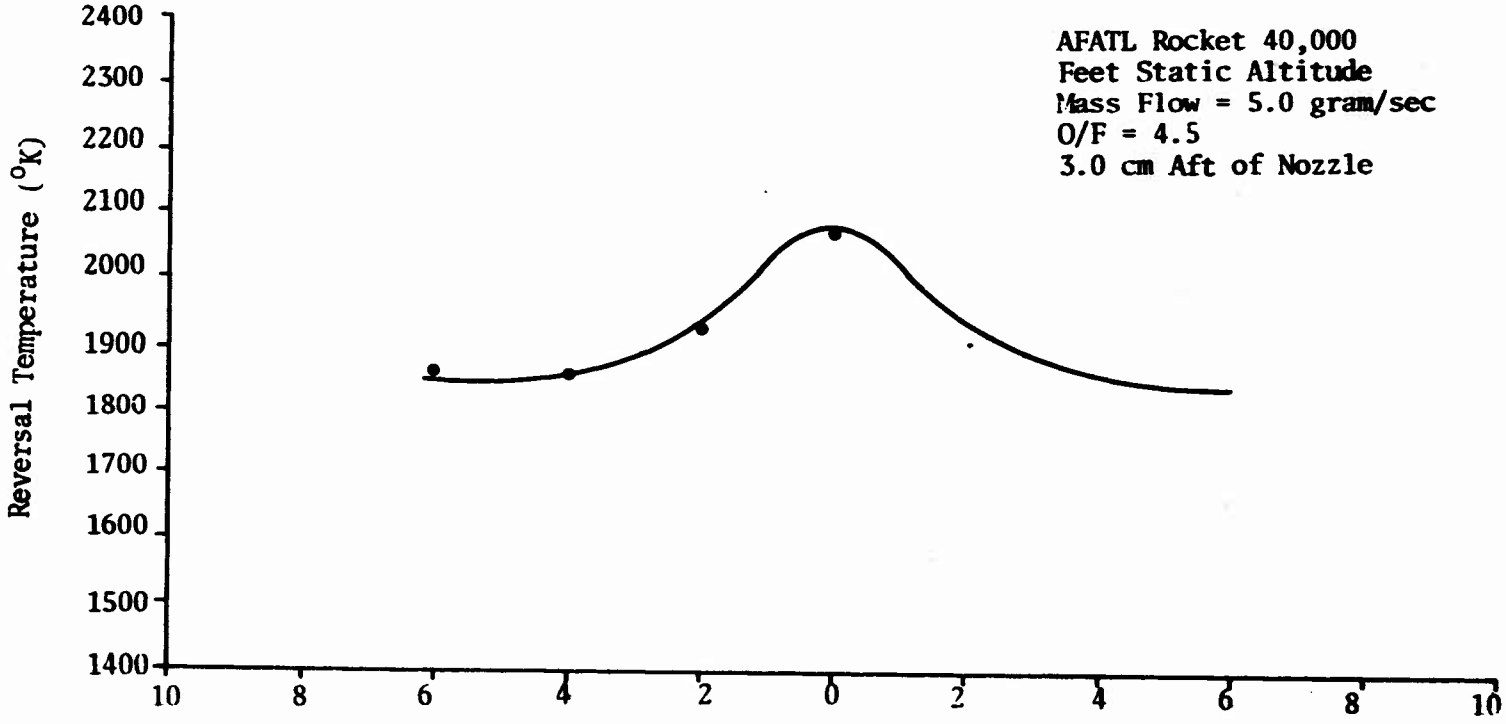

Figure C-4. Radial Temperature Scan (3.0 cm Aft of Rocket Nozzle)

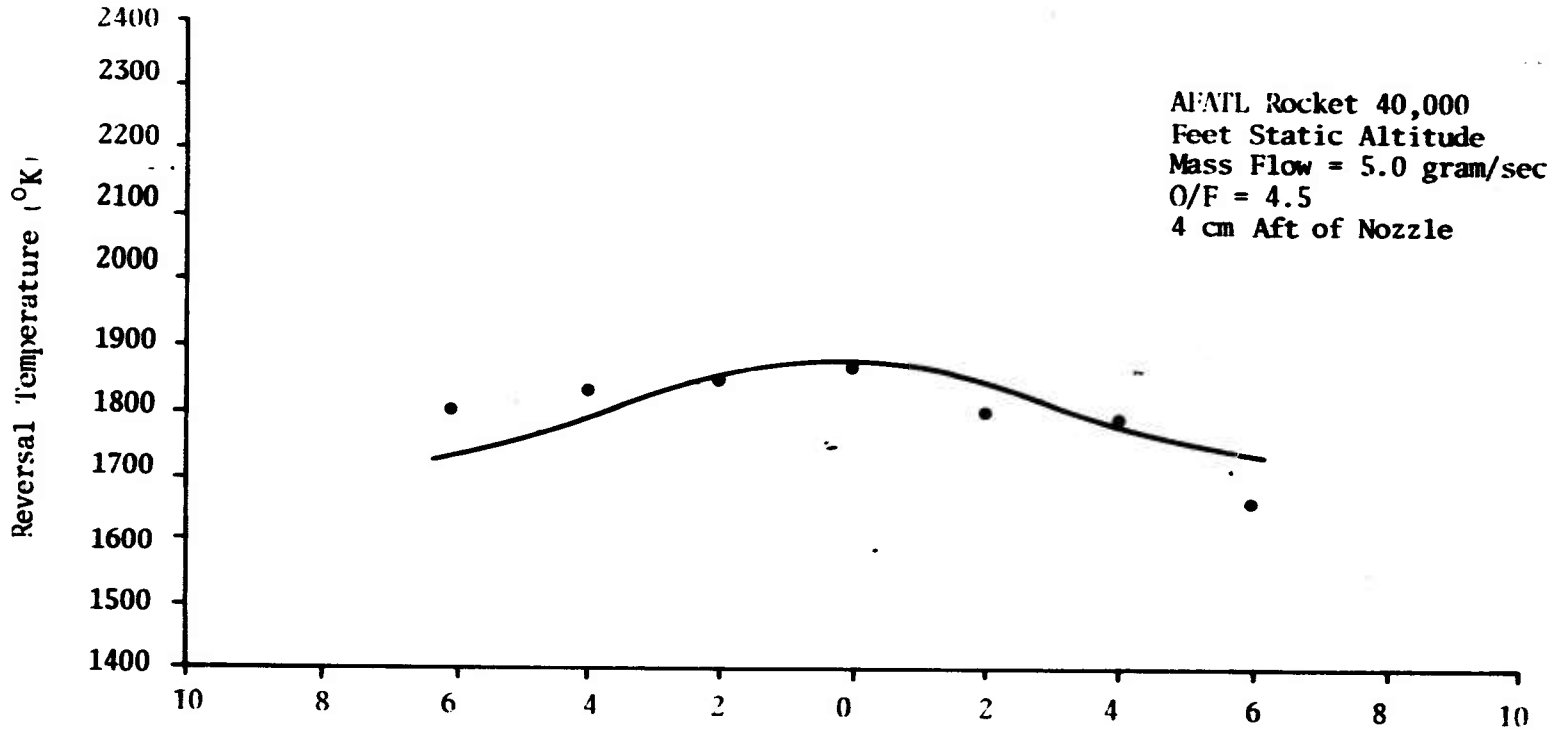

Figure C-5. Radial Temperature Scan (4 cm Aft of Rocket Nozzle)

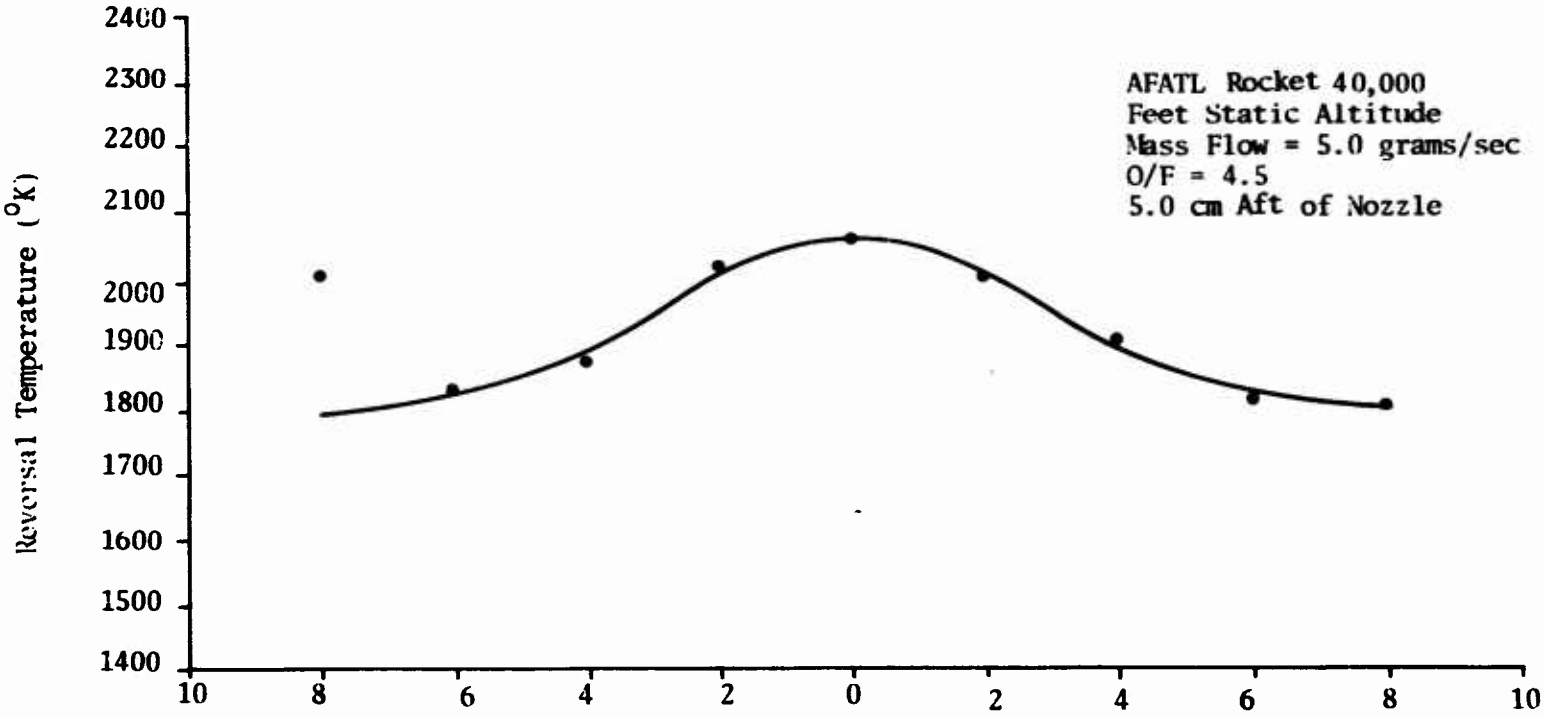

Figure C-6. Radial Temperature Scan (5.0 cm Aft of Rocket Nozzle)

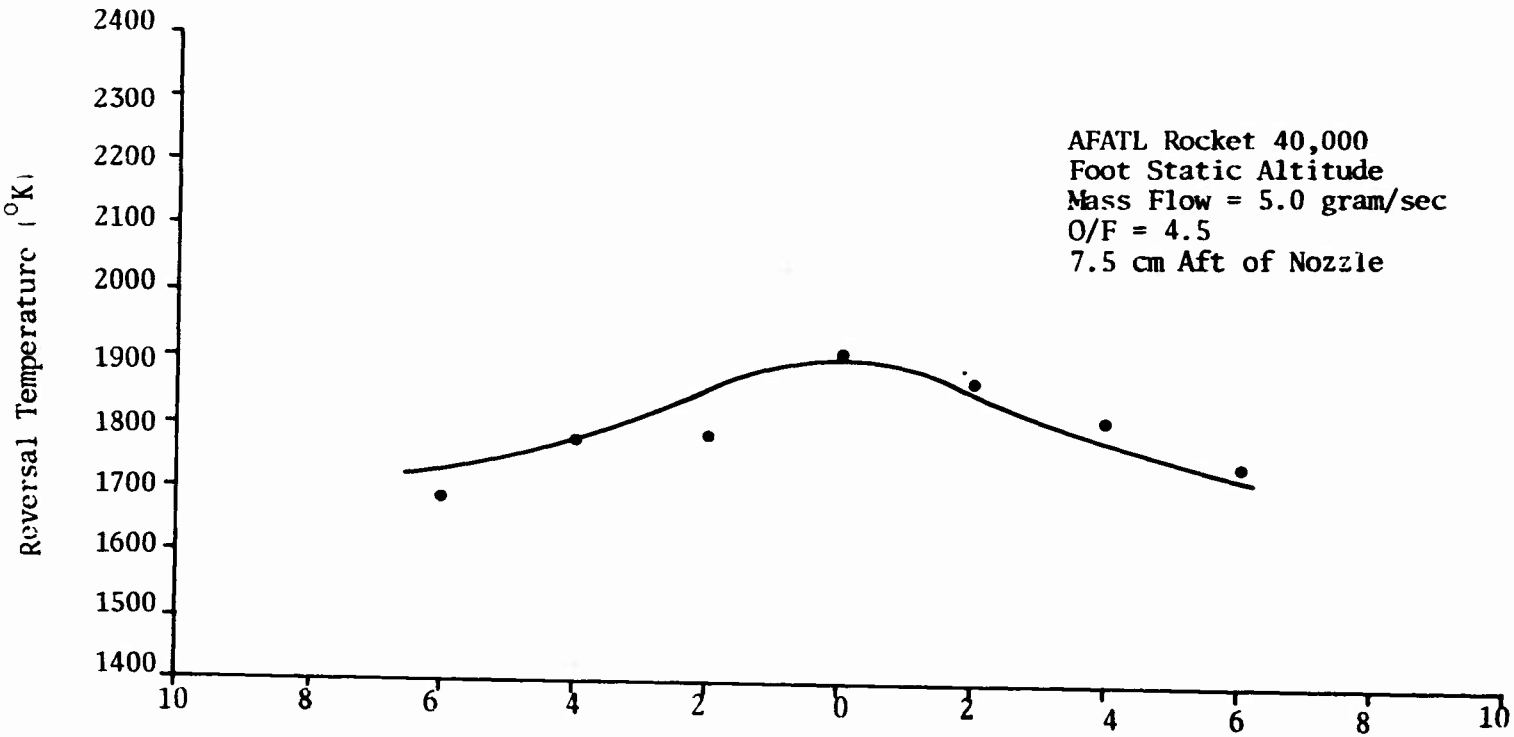

Figure C-7. Radial Temperature Scan (7.5 cm Aft of Rocket Nozzle)

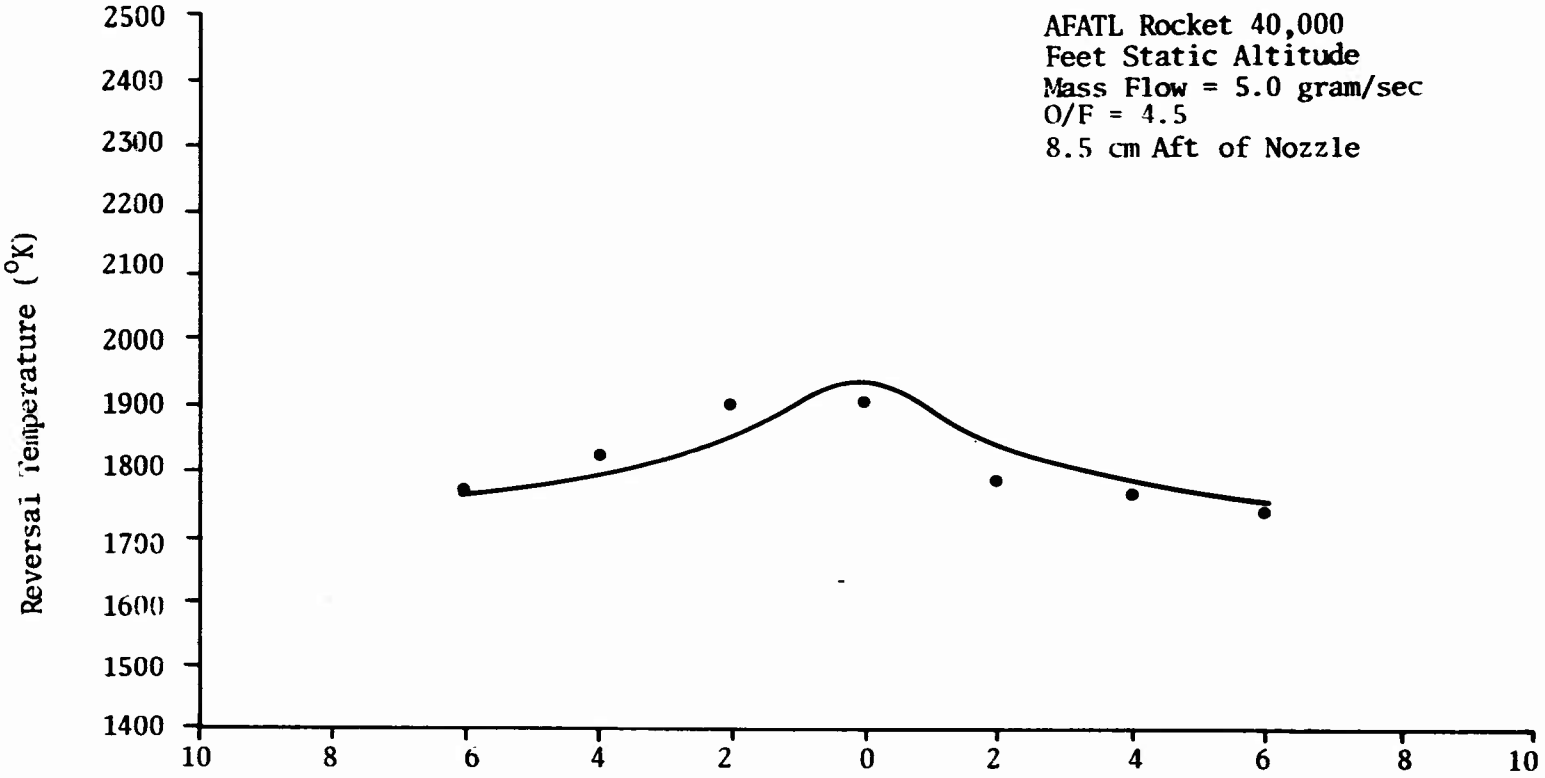

Figure C-8. Radial Temperature Scan (8.5 cm Aft of Rocket Nozzle)

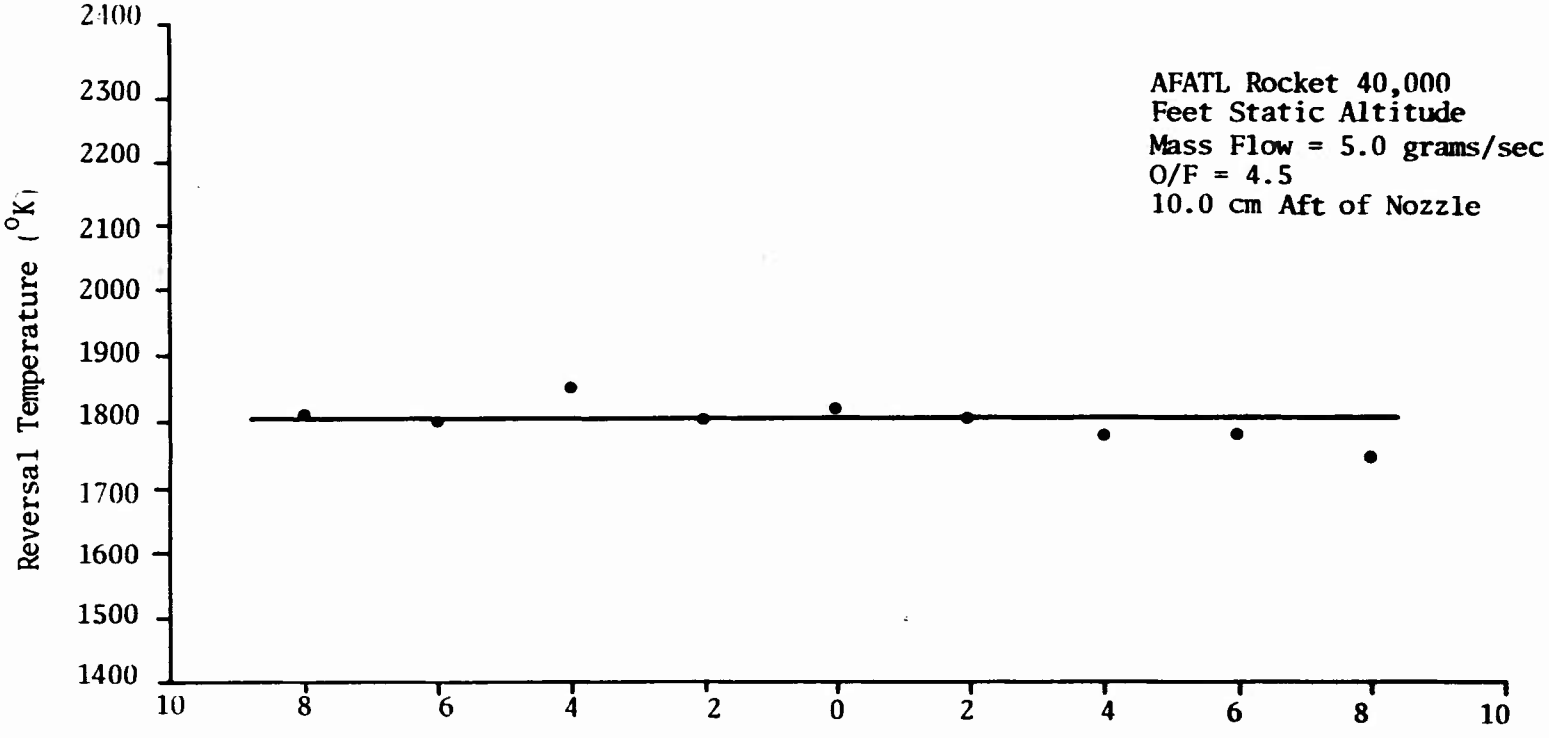

Figure C-9. Radial Temperature Scan (10.0 cm Aft of Rocket Nozzle)

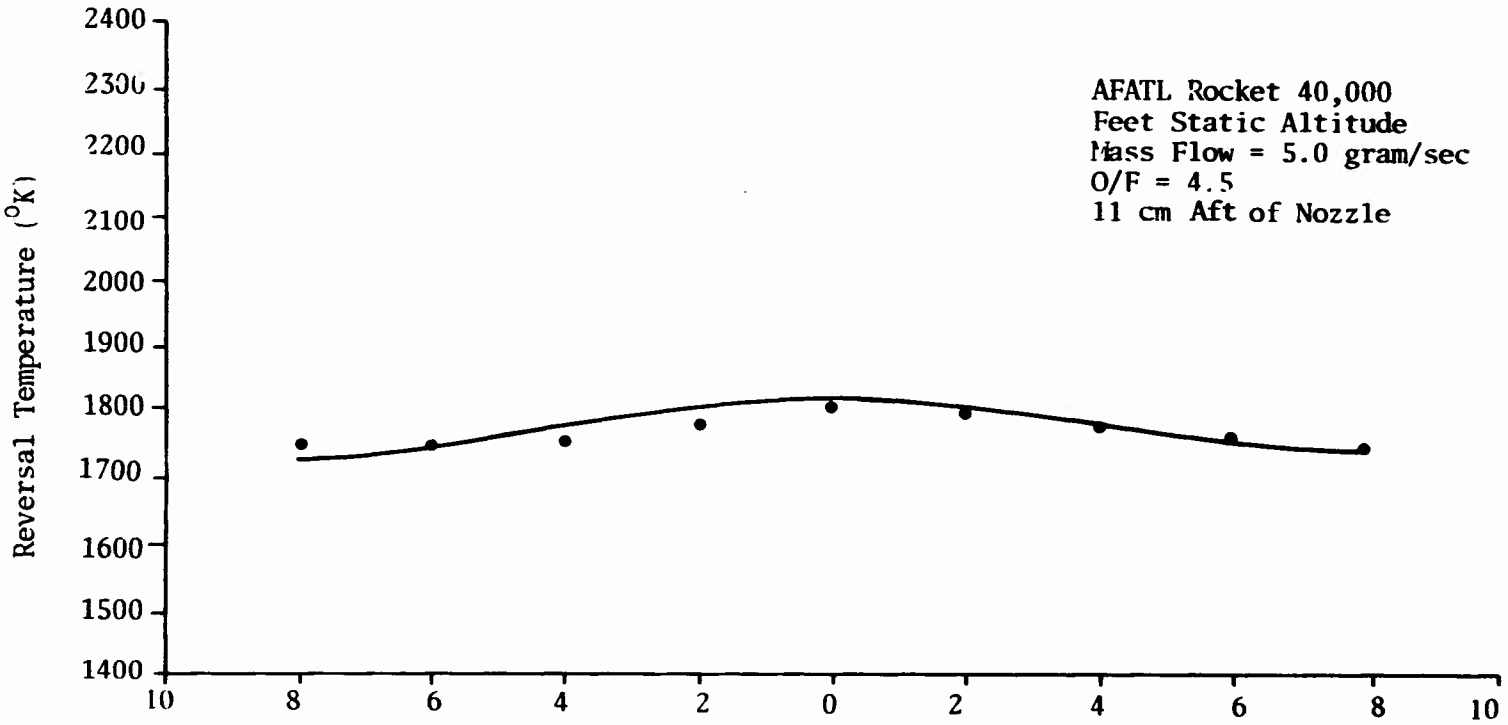

Figure C-10. Radial Temperature Scan (11 cm Aft of Rocket Nozzle)

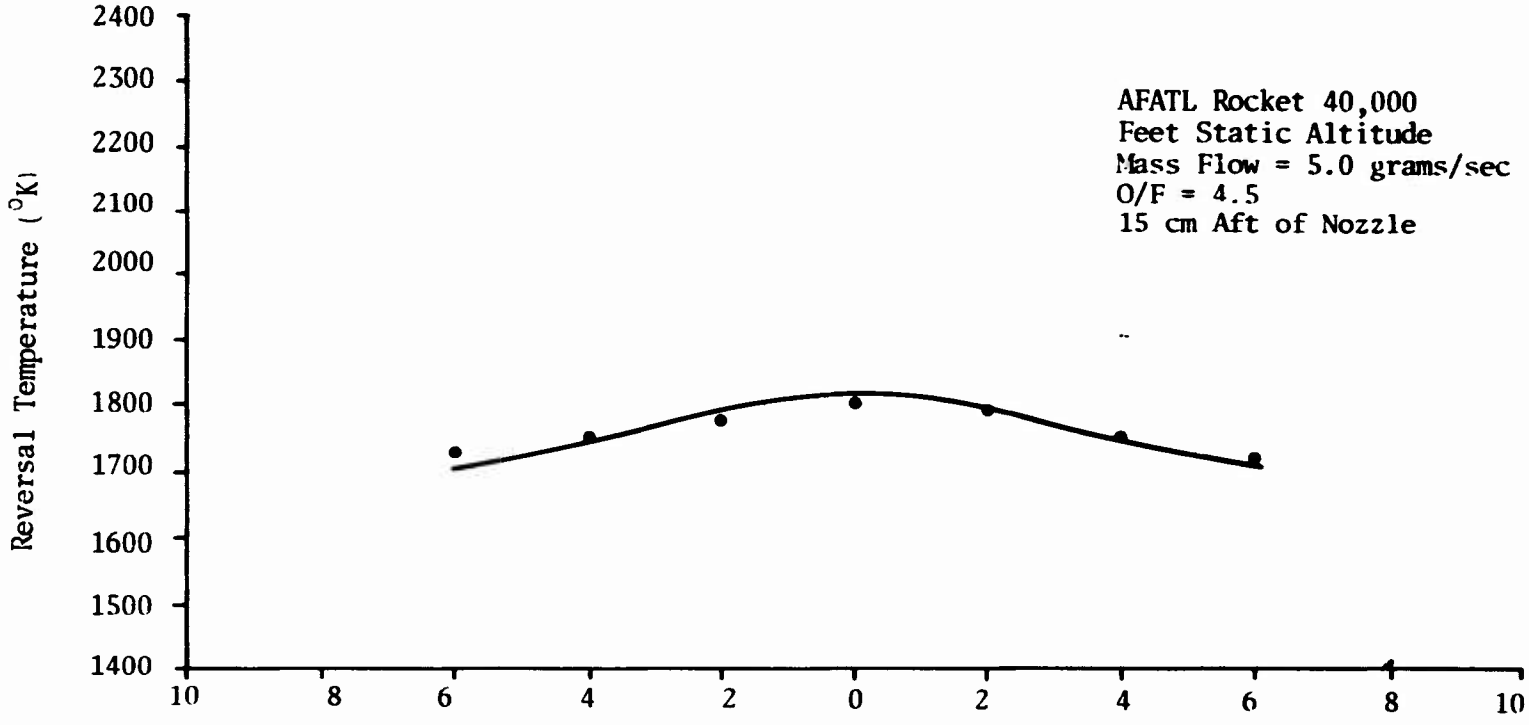

Figure C-11. Radial Temperature Scan (15 cm Aft of Rocket Nozzle)

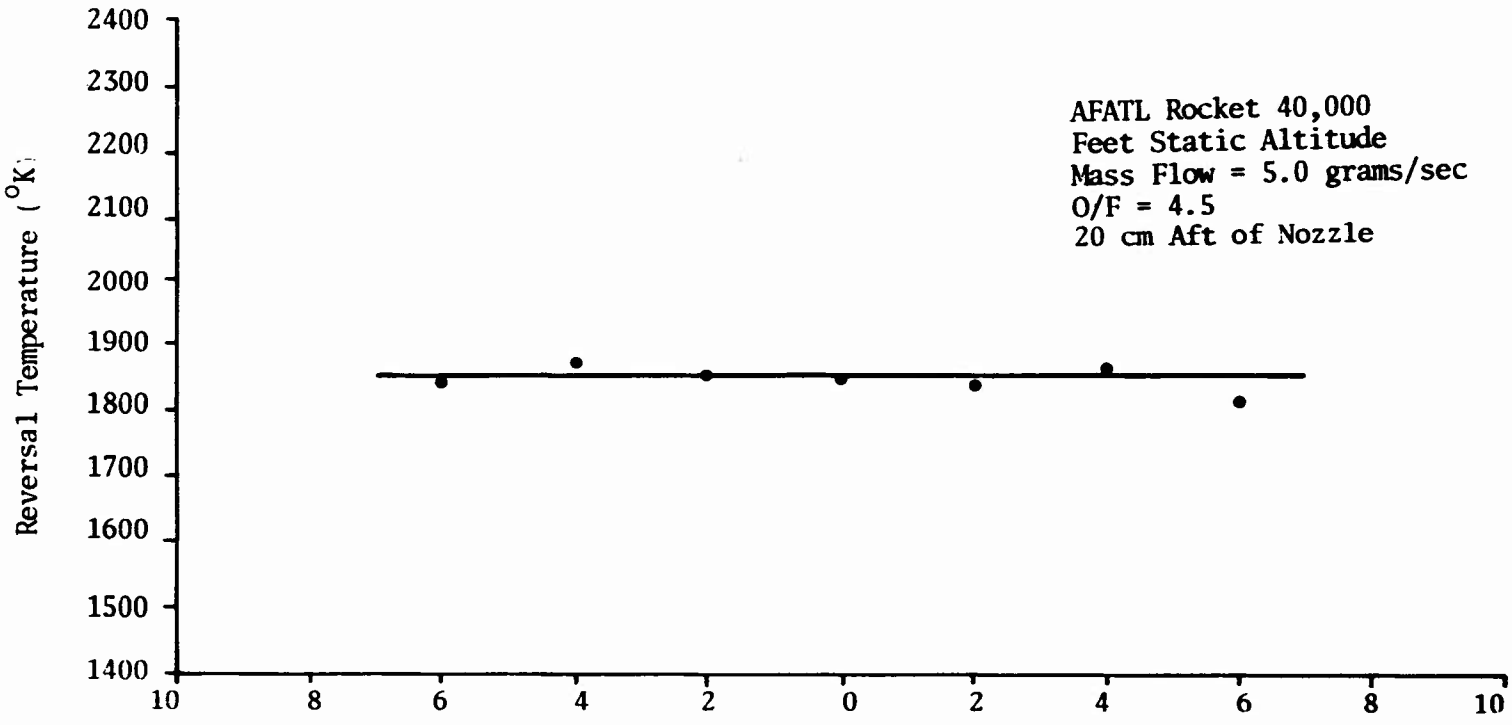

Figure C-12. Radial Temperature Scan (20 cm Aft of Rocket Nozzle)

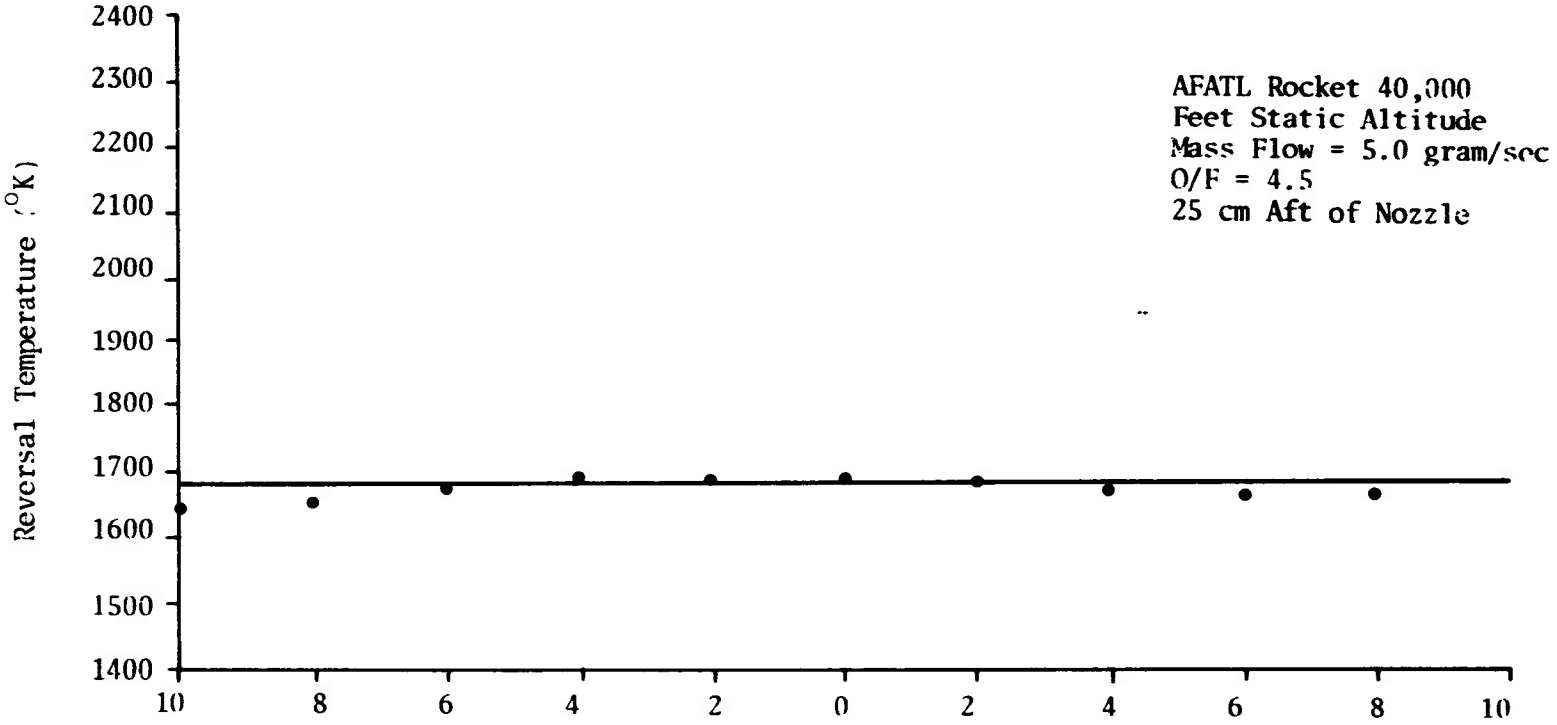

Figure C-13. Radial Temperature Scan (25 cm Aft of Rocket Nozzle)

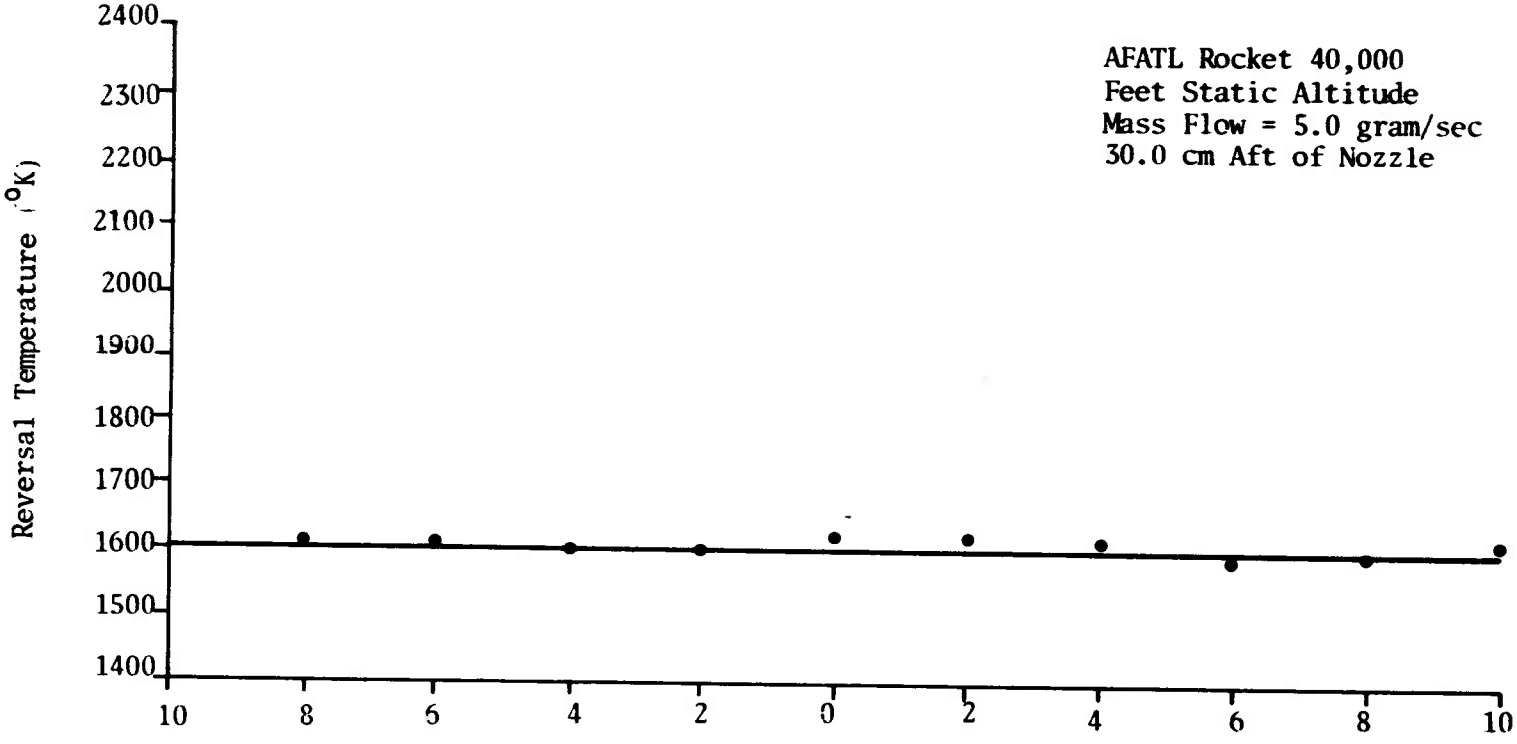

Figure C-14. Radial Temperature Scan (30.0 cm Aft of Rocket Nozzle)

(The reverse of this page is blank)

INITIAL DISTRIBUTION

HQ, USAF/SAMI	1	ODDR&E/TST&E	1
HQ USAF/RDPA	1	DARPA/TIO	1
HQ USAF/RDQRM	1	NAVAIR SYS COMD	1
HQ USAF/XOOFA	1	USAF/AFSC LIASON OFFICE	6
AFSC/INA	1	COMMANDER NWC/CODE 456	2
AFSC/SDA	1	COMMANDER NWC/CODE 533	1
AFSC/DLCAW	1	COMMANDER NWC/CODE 4063	1
AFIS/INT	1	COMMANDER NWC/CODE 40903	3
AFSC/DPSL	1	COMMANDER NWC/CODE 3301	1
AFSC/SDWM	1	COMMANDER NWC/CODE 335	1
TAC/DRA	2	REDSTONE SCI INFO CEN	3
TAC/XPSY	1	USN WEAPONS LAB (MAL)	1
AFAL/AA	1	CG USAMICOM	1
AFAL/TEM	1	DDC-TC	2
AFAL/RWM	1	CINCPACAF/IGFW	1
AFAL/RW	3	ADTC/PP	1
ASD/YHEV	1	ADTC/TE	1
ASD/XRG	2	ADTC/XR	2
ASD/YFEI (ARMAMENT)	1	SOF/DR	1
ASD/ENO	1	TAWC/ERW	1
ASD/ENYW	1	TAWC/TX	1
ASD/ENASA	1	AFATL/DL	1
ASD/YPEX	1	AFATL/DLB	1
ASD/RWS	11	AFATL/DLMI	5
ASD/RWR	2	AFATL/DLMM	1
ASD/ENFEA	1	AFATL/DLOU	1
ASD/SD (TECH DIR)	1	AFATL/DLY	2
ASD/SD7	2	AFATL/DLYA	1
ASD/SD5EI	1	AFATL/DLYW	1
ASD/SD4T	2	AFATL/DLJ	1
AFFDL/FE	1	AFATL/DLJF	1
AFFDL/FGL	1	AFATL/DLJC	1
AFFDL/FX	1	AFATL/DLJA	1
AFFDL/FY	1	AFATL/DLODL	2
AFML/MX	1	ADTC/SD	1
AFML/LL	1	ADTC/SDM	1
AFML/MB	1	ADTC/SDE	3
AFML/LP	1	ADTC/SD7	3
AFLC/MMWM	1	ASD/SDO	1
OO-ALC/MMWMP	2	ASD/SDM	1
6585 TG/GDP	1	AFFDL/FGC	1
AUL/LSE 71-249	1	AFML/LPO	1
ATC/XPQS	1	USAF ACADEMY	1
NAV AIR SYSTEMS COMD/AIR-5323	1	SAC/XHHN	2
NAV AIR SYSTEMS COMD/AIR-5324	1	SAC/DOXT	1

SAC/LGWC	1
AFAL/NVA-679A	2
ASD/SD-65	1
TAWC/TXA	1
PHILCO-FORD	1
ROCKWELL INTERNATIONAL	1
HUGHES AIRCRAFT CO.	1
MARTIN-MARIETTA	1
RAND CORPORATION	1
AFRPL/MK	1
GENERAL DYNAMICS	1
TAC/INAT	1
ASD/XRP	1
HQ USAFE/DOQ	1
USA TRADOC SYS ANALYS ACTVY	1
HQ PACAF/DOOFQ	3
COMIPAC/I-232	1
ASD/ENESS	1